Influence of Gaze Rotation on the Visual Response of Primate MSTd Neurons

KRISHNA V. SHENOY, DAVID C. BRADLEY, AND RICHARD A. ANDERSEN
Division of Biology, California Institute of Technology, Pasadena, California 91125

Shenoy, Krishna V., David C. Bradley, and Richard A. Andersen. Influence of gaze rotation on the visual response of primate MSTd neurons. *J. Neurophysiol.* 81: 2764–2786, 1999. When we move forward, the visual image on our retina expands. Humans rely on the focus, or center, of this expansion to estimate their direction of heading and, as long as the eyes are still, the retinal focus corresponds to the heading. However, smooth rotation of the eyes adds nearly uniform visual motion to the expanding retinal image and causes a displacement of the retinal focus. In spite of this, humans accurately judge their heading during pursuit eye movements and during active, smooth head rotations even though the retinal focus no longer corresponds to the heading. Recent studies in macaque suggest that correction for pursuit may occur in the dorsal aspect of the medial superior temporal area (MSTd) because these neurons are tuned to the retinal position of the focus and they modify their tuning during pursuit to compensate partially for the focus shift. However, the question remains whether these neurons also shift focus tuning to compensate for smooth head rotations that commonly occur during gaze tracking. To investigate this question, we recorded from 80 MSTd neurons while monkeys tracked a visual target either by pursuing with their eyes or by vestibulo-ocular reflex cancellation (VORC; whole-body rotation with eyes fixed in head and head fixed on body). VORC is a passive, smooth head rotation condition that selectively activates the vestibular canals. We found that neurons shift their focus tuning in a similar way whether focus displacement is caused by pursuit or by VORC. Across the population, compensation averaged 88 and 77% during pursuit and VORC, respectively (tuning shift divided by the retinal focus to true heading difference). Moreover the degree of compensation during pursuit and VORC was correlated in individual cells ($P < 0.001$). Finally neurons that did not compensate appreciably tended to be gain-modulated during pursuit and VORC and may constitute an intermediate stage in the compensation process. These results indicate that many MSTd cells compensate for *general* gaze rotation, whether produced by eye-in-head or head-in-world rotation, and further implicate MSTd as a critical stage in the computation of heading. Interestingly vestibular cues present during VORC allow many cells to compensate even though humans do not accurately judge their heading in this condition. This suggests that MSTd may use vestibular information to create a compensated heading representation within at least a subpopulation of cells, which is accessed perceptually only when additional cues related to active head rotations are also present.

INTRODUCTION

Visual motion provides primates with a wealth of information about where objects are and how they move. In many situations, however, visual motion alone is ambiguous because only relative motions are seen. For example, rightward motion in the retinal image could be caused either by an object moving to the right or by a turn of the eyes or head to the left. In these situations, the visual system must rely on extraretinal signals containing information about eye and head movement to interpret visual motion correctly. Although a great deal is known about the neural structures that interpret visual motion when the gaze is fixed (Maunsell and Newsome 1987) as well as about the neural mechanisms that integrate visual and gaze-position signals (Andersen 1997), much less is known about motion processing during eye and head rotations.

How does the brain combine visual-motion and extraretinal gaze-rotation signals? We considered this question in the context of visual navigation (Gibson 1950; Warren 1995). When we move forward, the retinal image expands. The center or focus of this expansion (FOE) corresponds to the heading, or instantaneous direction of translation, when the gaze is fixed, and humans can use the FOE to estimate accurately their heading (Warren and Hannon 1988). However, when we smoothly shift our gaze, as during pursuit eye movements, the FOE on the retina is displaced from the true heading as illustrated in Fig. 1. Humans use an extraretinal pursuit signal to compensate for this displacement and, thereby, are able to judge their heading quite accurately even during pursuit (mean compensation of 90%) (Crowell et al. 1998a; Royden et al. 1992, 1994).

We recently reported that many neurons in macaque extrastriate cortical area MSTd (dorsal subdivision of the medial superior temporal area) use pursuit signals to compensate, at least partly, for the displacement of the FOE caused by pursuit eye movements (Andersen et al. 1996; Bradley et al. 1996). MSTd is well suited for such visual and nonvisual cue integration, which is essential for estimating heading, because of the following receptive field specializations and extraretinal contributions: 1*)* large receptive fields (RFs) (often >50° in diameter); *2*) selectivity for the direction of laminar motion; *3*) selectivity for expansion, contraction, rotation, or spiral optic-flow patterns (Duffy and Wurtz 1991a,b; Graziano et al. 1994; Komatsu and Wurtz 1988a,b; Lagae et al. 1994; Lappe et al. 1996; Orban et al. 1992; Raiguel et al. 1997; Saito et al. 1986; Sakata et al. 1985, 1994; Tanaka and Saito 1989; Tanaka et al. 1986, 1989); *4*) optic-flow selectivity is typically invariant to the position of the pattern within the RF (Duffy and Wurtz 1991b; Graziano et al. 1994; Lagae et al. 1994; Orban et al. 1992); *5*) optic-flow selectivity does not depend on the forms or cues of the moving objects (Geesaman and Andersen 1996); *6*) optic-flow selectivity is typically invariant to the size of the visual pattern (Graziano et al. 1994); *7*) responses are modu-

The costs of publication of this article were defrayed in part by the payment of page charges. The article must therefore be hereby marked ''*advertisement*'' in accordance with 18 U.S.C. Section 1734 solely to indicate this fact.

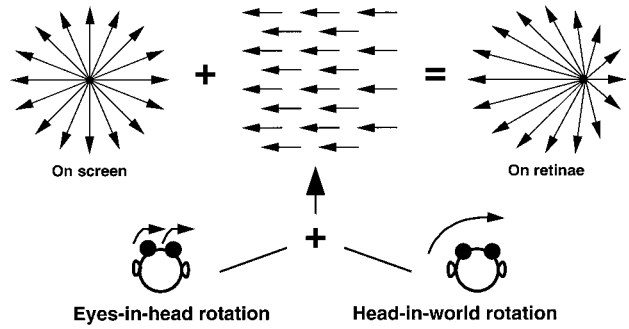

FIG. 1. Retinal image while moving forward and rotating gaze. When we move forward and hold our eyes still, the visual motion pattern (optic flow) on our retinae is radial expansion; focus of expansion (FOE) position indicates the heading. We recreated this retinal image motion on a computer screen (on screen). When we move forward but now rotate our eyes in our head or our head in the world, to track an object moving to the right for example, leftward rotational flow is added to the retinal image (on retinae). Rotational flow displaces the FOE to the right. Without correction, this displacement leads to large errors in self-motion estimates.

lated by the position of the FOE in the RF (Duffy and Wurtz 1995); *8*) responses are modulated by the rate of optic-flow expansion (Duffy and Wurtz 1997); *9*) responses are modulated by stereoscopic disparity (Roy and Wurtz 1990; Roy et al. 1992); *10*) smooth-pursuit signals are direction and speed tuned (Bradley et al. 1996; Erickson and Thier 1991; Kawano et al. 1984, 1994; Newsome et al. 1988); and *11*) eye-position signals are present (Bremmer et al. 1997; Squatrito and Maioli 1996; Squatrito et al. 1997). Finally a recent report that microstimulating expansion-selective columns in macaque MSTd systematically biases heading estimates provides direct evidence that MSTd neurons contribute to the visual sensation of heading (Britten 1998; Britten and van Wezel 1998, Celebrini and Newsome 1995; Geesaman et al. 1997).

The question remains whether MSTd neurons also shift focus tuning to compensate for FOE displacements caused by smooth head rotations, which commonly occur during gaze tracking (see Fig. 1). Recent human psychophysical experiments indicate that self-motion judgments are quite accurate during active, smooth head rotations (observers smoothly rotate their heads while fixating a target moving with the head; mean compensation of 94%) (Crowell et al. 1998a). In this condition, there are three sources of extraretinal information that potentially drive compensation: proprioceptive information from the neck muscles, efferent information about the motor commands sent to the neck muscles, and vestibular canal information about head rotation.

As a first step, we asked if vestibular canal signals contribute to MSTd focus-tuning compensation during head-in-world rotations, as pursuit signals contribute to focus-tuning compensation during eye-in-head rotations. We suspected canal signals in MSTd because otolith signals recently were found in MSTd (Duffy 1998) and because canal signals have been reported in MSTl and in nearby areas of the posterior parietal cortex (Kawano et al. 1980, 1984; Sakata et al. 1994; Snyder et al. 1998; Thier and Erickson 1992a,b). To investigate this question, we trained two monkeys to perform a vestibulo-ocular reflex cancellation (VORC) task in which we mechanically rotated their bodies and heads while they fixated a target rotating with their bodies and heads. The eyes rotate in the world, but not in the head, during VORC. By measuring the response of MSTd cells to optic-flow patterns during both VORC and fixed gaze conditions, we could assess vestibularly induced focus tuning shifts. We found substantial focus tuning compensation during VORC. Interestingly although vestibularly-derived signals are essential for accurate self-motion estimates during active, smooth head rotation (Crowell et al. 1998a), humans do not judge their self-motion accurately during the VORC task where the only extraretinal signal available is vestibular in origin (mean compensation of 4%) (Crowell et al. 1998a). MSTd physiology results are compared with human psychophysical performance in the DISCUSSION.

The oculomotor mechanisms engaged during VORC are not well understood. There appear to be three possibilities. First, during VORC the vestibular ocular reflex (VOR) could be shut down, thereby allowing fixation of the VORC target without any eye movement commands. Second, it is possible that the VOR is active during VORC and that a pursuit signal is generated to oppose the VOR signal, thereby enabling VORC-target fixation. Finally a combination of these mechanisms could underlie VORC-task performance. Recordings from the brain stem appear to implicate both ocular and vestibular sources of VORC signals, consistent with this last possibility (Cullen and McCrea 1993; Cullen et al. 1991, 1993; Tomlinson and Robinson 1984). Posterior parietal cortex (PPC) studies also appear to be consistent with this view. Robust responses have been reported in MSTl, the lateral subdivision of MST, during sinusoidal VORC (Thier and Erickson 1992a,b). These responses persisted, though at roughly half the strength, during sinusoidal rotation in complete darkness, which isolates the vestibular canal component of the signal. Regardless of the exact origin, VORC signals are present naturally during tracking head movements and are viable extraretinal cues for heading estimation.

Brief reports of this material have appeared previously (Shenoy et al. 1996, 1997).

METHODS

Animal preparation

Experiments were conducted in two hemispheres of two adult, male Rhesus monkeys (*Macaca mulatta*), and all protocols were approved by the Caltech Institutional Animal Care and Use Committee. In a sterile surgical procedure under sodium pentabarbitol anesthesia, stainless steel bone screws were implanted in the skull, and a fixture for immobilizing the head was constructed with methylmethacrylate. In the same procedure, a Teflon-insulated, 50-gauge stainless steel wire coil was implanted between the conjuctiva and the sclera for the measurement of eye position (Judge et al. 1980; Robinson 1963). The coil was connected electrically to a coaxial connector embedded in the methylmethacrylate.

Behavioral training on oculomotor tasks began no sooner than 1 wk after surgery. Monkeys received juice rewards for correct performance during both behavioral training and experimental sessions. Adequate performance levels, typically >90% on all tasks, were reached after several weeks of training. A subsequent surgery was performed to open a craniotomy and to implant a Lucite cylinder (5 mm posterior, 17 mm lateral, dorsoventral orientation), which provided chronic access to cortical area MSTd for electrophysiological recording.

Recording techniques

Extracellular action potentials were monitored with varnish-coated tungsten microelectrodes, with ~1 MΩ impedance at 1 kHz. A

stainless steel guide tube was advanced manually dorsoventrally through the dura and the electrode was extended further into the brain with a hydraulic micropositioner. Action potentials were amplified and single neuron waveforms were isolated with a time-voltage discriminator. MSTd was identified based on the following criteria: *1*) depth below the dura; *2*) position relative to gray and white matter boundaries; *3*) location relative to the middle temporal (MT) cortical area; *4*) receptive field size (typically >50° diam with both contra- and ipsilateral visual responses); *5*) selectivity for optic-flow type (e.g., expansion); and *6*) position invariance of optic-flow selectivity within the receptive field. Neurons tuned for the type of optic flow, by visual inspection and in at least one location in the RF, were tested in all experiments and are included in our database. Action potential event times and behavioral states were stored for subsequent analysis.

Visual stimuli

All experiments were conducted in a sound-insulated room, which was totally dark except for the visual stimuli. We generated expanding random dot optical flow fields by simulating forward translation at 16.5 cm/s toward a fronto-parallel wall held 38.1 cm distant. One thousand dots were placed randomly in computer memory representing an 82 × 82° area, and each dot was assigned a random age. Dots moved at constant velocity for the remainder of their 300-ms lifetime or until they crossed the area perimeter, in which case they were extinguished and reborn at a random location. Dot speeds were proportional to the eccentricity from the FOE, reaching 9.2°/s at 24° eccentricity. The direction of dot motion was rotated by 90, 180, or 270° from the expansion stimuli to create counterclockwise rotation, contraction, or clockwise rotation stimuli, respectively. Dots were white (~10 candela/m^2) on a completely black background and were not anti-aliased. Displays were viewed binocularly.

We displayed an 18 × 18° subregion (window) of the total area simulated on a computer monitor operating in 640 × 480 pixel resolution and 60 frames/s mode. This was the largest possible stimulus area due to monitor size (50 × 38° at 38.1 cm), monitor weight (the monitor moved with the vestibular chair), stimulus movement, and stimulus position constraints. Such display windows contained 48 dots (0.15 dots/deg^2) with each dot subtending 0.08 × 0.08° of visual angle (1 pixel). Display windows, including the optic flow and the invisible window frame, were presented: at a fixed location in the room, moving with the fixation target, which moved in the room, or drifting across the room (see *Behavioral tasks*).

Pursuit targets moved an integral number of pixels/frame resulting in smooth motion (e.g., 2 pixels/frame = 9.2°/s); consequently, horizontal and vertical pursuit targets moved at 9.2°/s while 45° diagonal pursuit targets moved $\sqrt{2}$ times faster. Fixation and VORC targets remained stationary on the display, but during VORC trials the entire display moved at 9.2°/s or $\sqrt{2}$ times faster for diagonal trials. The direction and speed of pursuit- and VORC-tracking targets were identical in all experiments. Fixation, pursuit, and VORC targets subtended 0.24 × 0.24° of visual angle.

To simulate different headings, we created nine optic-flow patterns with varying focus (origin) positions by shifting the origin of the 82 × 82° pattern behind the 18 × 18° window (aperture). Focus positions varied from −32 to 32° in 8° increments along an axis either parallel to the neuron's preferred-null axis (see *Data analysis*) for expansion/contraction neurons, or orthogonal to this axis for rotation neurons. Different axes are required because the direction of origin shift depends on both the visual pattern and on the direction of gaze rotation (Andersen et al. 1996; Bradley et al. 1996). For example, rightward pursuit across an expansion pattern shifts the focus rightward (parallel to pursuit), whereas rightward pursuit across a clockwise rotation pattern shifts the origin of rotation upward (orthogonal to pursuit). Diagonal focus spacing and range was increased by $\sqrt{2}$ to account for the $\sqrt{2}$ increased real and simulated gaze-tracking speeds during diagonal trials.

We selected the gaze rotation and display parameters described above to shift the focus (origin) during gaze rotation by 24°. Physical geometry and gaze rotation lead to the following governing equations:

$$\dot{\theta} = \frac{x}{z^2 + x^2} \cdot T_z \quad \text{and} \quad \tan(\theta) = \frac{x}{z} \tag{1}$$

where θ (rads) is the visual angle to a particular point on the simulated wall that the observer is approaching, $\dot{\theta}$ (rads/s) is the rate at which θ increases, x (cm) is the linear distance from the center of the wall to the point being considered, z is the distance from the observer to the wall (38.1 cm), and T_z is the simulated forward translation speed of the observer (16.5 cm/s). Substituting the experimental parameters into these equations reveals that a point on the simulated wall 24° eccentric travels outward at a speed of 9.2°/s. Therefore when the eyes rotate at 9.2°/s, the point 24° eccentric does not move on the retinae, which is the definition of a focus (origin). Thus the focus (origin) shifts 24° during gaze rotation as compared with when the eyes are still (focus at 0°). To detect tuning curve shifts smaller than the theoretical shift during gaze rotation (24°), we spaced the foci (origins) every 8° to generate tuning curves with sufficient sampling resolution.

Vestibular stimuli

Monkeys were seated comfortably in a primate chair which we attached to a vestibular chair (Acutronic, Pittsburgh, PA). Precise horizontal plane (yaw) and sagittal plane (pitch) rotations were executed by the feedback control system. Vestibular chair sensors reported real-time position information, which was monitored and used to trigger visual stimulus onsets during VORC trials. We fixed the monkeys' heads to the primate chair such that the axis of yaw rotation passed through the midline (medial/lateral), midway between the ear canals and the center of the eyes (anterior/posterior). The pitch rotation axis was positioned midway between the ear canals and the center of the eyes (anterior/posterior), in the plane of the ear canals and the center of the eyes (dorsal/ventral). This arrangement is intermediate between the natural eye rotation axes, passing roughly through the center of the eyes, and the natural head rotation axis, passing through the neck. This compromise produces rotations that approximate natural head rotations but without creating excessive visual translation during VORC conditions, which is not present during eye pursuit.

A computer monitor and electromagnets also were mounted on the vestibular chair. The electromagnetic coils were attached to the vestibular chair to improve eye position accuracy by maintaining a more uniform local magnetic field during large-angle body rotations. Even with such measures, it was not possible to maintain a perfectly constant magnetic field because the position and orientation of various vestibular chair components in the magnetic fringe fields changed through the course of a vestibular chair rotation. The resulting systematic drift in eye position measurement over the range of vestibular chair rotations (±20° yaw and/or pitch) was ~1° and was substantially <1° over the smaller rotation range traveled during visual stimulus presentation and data collection (±4.6° yaw and/or pitch).

Although the on-line eye position tolerance (demand box) was enlarged slightly to account for this variation (typically ±4° square), inspection of the eye traces revealed accurate pursuit (very few, small catch-up saccades), accurate VORC (very few, small VOR/OKN drifts), accurate simulated gaze rotation (fixation), and accurate fixed gaze (fixation). Off-line analysis consisted of selecting 16 heading experiments at random, 8 from each monkey and totalling 20% of all heading experiments, and calculating the deviation of the eye from the average fixation position (simulated gaze rotation and fixed gaze trials), from the average VORC position (VORC trials), or from a line regressed through the eye trace (pursuit trials). The average standard deviation across all trials was quite small in all conditions: horizontal (0.31°) and vertical (0.32°) channel VORC, horizontal (0.30°) and

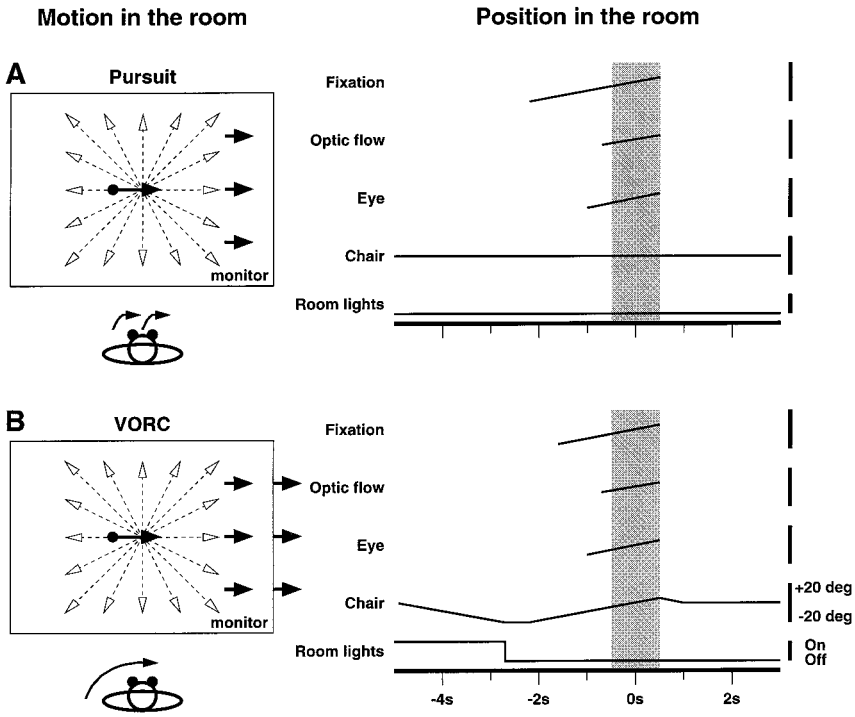

FIG. 2. Schematic illustrations and timing diagrams for the 2 behavioral tasks in the preferred-direction experiment. Rightward gaze rotation conditions are shown in this example, although gaze rotations in 8 directions in the fronto-parallel plane were performed in the experiment. *Left*: all arrows refer to movement in the room and indicate conditions during the data-collection interval. *A*: pursuit task requires pursuing a moving target (filled circle with filled arrow) while viewing the preferred optic flow stimulus (e.g., expansion; dashed motion vector arrows) which moves with the pursuit target (3 filled arrows). *B*: vestibulo-ocular reflex cancellation (VORC) task requires fixating a target moving in register with the head and body while viewing the preferred-optic-flow stimulus that moves with the fixation target. *Right*: timing diagrams plot the experimental conditions and behavioral requirements as a function of time. Lines represent physical positions in the room, hence parallel lines indicate no relative movement (only horizontal and yaw positions are shown for simplicity). Presence of a line indicates the presence of a stimulus (fixation and optic flow) or a positional requirement being enforced (eye and vestibular chair). For room lights, the line position indicates the light status. Times are aligned on the middle (0.0 s) of the 1.0-s data-analysis period, shown in gray. Onset times for pursuit trials are as follows: −700 ms, optic-flow stimulus; −1.0 s, proper eye position required; and −2.2 s, fixation target appears. Onset times for VORC trials are as follows: −700 ms, optic-flow stimulus; −1.0 s, proper eye position required; −1.6 s, fixation target appears; and −2.2 s, chair begins sweep. At −2.7 s, the chair arrives at the ready position and the room lights are extinguished.

vertical (0.31°) channel pursuit, horizontal (0.18°) and vertical (0.30°) channel simulated gaze rotation, and horizontal (0.18°) and vertical (0.30°) channel fixed gaze.

We reproduced the retinal image seen during pursuit by generating head, body, and eye rotations using the VORC paradigm. Both pursuit and VORC conditions require an ~2 s constant angular rotation period (9.2°/s, $\sqrt{2}$ times faster during combined yaw and pitch rotations), during which time the visual stimulus is displayed and neural data are collected. This constant angular velocity period was embedded in the middle of a trapezoidal speed trajectory: 307 ms, 30°/s^2 constant acceleration phase; ~2 s constant velocity phase; and a 307 ms, 30°/s^2 deceleration phase. To verify that this protocol effectively generates VORC signals, we recorded the response of two representative MSTd neurons in a pursuit and VORC paradigm in which only a pursuit or VORC target was present and in which the constant rotation period lasted 4 s. Robust responses persisted out to ≥4 s in both conditions, indicating that the velocity signal, which is integrated from rotational acceleration cues by the vestibular canal apparatus and which ultimately drives the MSTd VORC signal, has a time constant of at least a few seconds (Wilson and Jones 1979).

Behavioral tasks

Monkeys were trained to perform three types of behavioral tasks: fixation, pursuit, and VORC. One or more of these behavioral tasks were employed in three sequential, blocked experiments: preferred optic flow, preferred direction, and heading.

Preferred-optic-flow experiment trials consist of fixating (less than ±2.5° eye box) a target for 1.7 s, during which time a 1.2-s optic-flow display appears. To determine the preferred type of optic flow, expansion, contraction, clockwise rotation, and counterclockwise rotation stimuli were presented pseudorandomly (stimuli randomly drawn without replacement and blocked by repetition number). Optic-flow stimuli were centered at 0°,0°; −10°,+10°; −10°,−10°; 10°,10°; and 10°,−10° (horizontal, vertical pairs; + indicates either ipsilateral or up) while gaze was fixed at 0°,0°. An additional configuration with gaze fixed at −10°,0° and optic flow centered at +15°,0° also was included to test for far ipsilateral responses. Receptive field sizes were estimated using this timing and hand-positioned patterns.

Preferred-direction experiment trials consist of pursuit or VORC of a moving target (9.2°/s or $\sqrt{2}$ faster) for 1.5 s, during which time a 1.2-s preferred-optic-flow display appears and moves with the target (less than ±4.0° eye box). Trial illustrations and timing diagrams are shown in Fig. 2. During VORC trials, the target remains fixed on the screen (screen moved with the vestibular chair), and there is no eye-in-head rotation (confirmed by monitoring eye position). Also there is nominally no head-on-body rotation, promoted by seating the monkeys comfortably and noting his relatively constant seating position in the primate chair (Lucite box). Eye pursuit and VORC trials were presented pseudorandomly (*monkey FTZ*) or blocked (*monkey*

DAL) in eight directions in the fronto-parallel plane (0, 45, . . . , 315°; 0° indicates eye rotation or chair yaw to the right; 90° indicates upward eye rotation or chair pitch). Gaze trajectories were centered on the same room location for both tasks to equalize all gaze angles on average. Gaze rotated by ±4.6° about the central location during the 1.0-s data-analysis period.

We presented and moved the preferred-optic-flow stimulus (e.g., expansion) along with the pursuit and VORC target in this experiment for two reasons. First, optic flow significantly increases the neural response and allowed us to better determine gaze-rotation directional tuning. Second, we sought to select the axis along which the gaze-rotation signal varies maximally. As long as the retinal stimulus is comparable between pursuit and VORC trials, the presence of a visual stimulus is acceptable. That the results of the heading experiment reported here are similar to the results we reported previously (Bradley et al. 1996), where a visual stimulus was not present during pursuit-axis selection, suggests that directional tuning largely is unaffected by the presence of the optic-flow pattern.

Heading experiment trials consist of fixation, pursuit or VORC of a target (less than ±4.0° eye box) for 1.5 s, during which time a 1.2-s preferred-optic-flow display appears. Nine optic-flow stimuli, with differing focus (origin) positions, and four behavioral tasks were presented pseudorandomly. Trial illustrations and timing diagrams are shown in Fig. 3. Pursuit and VORC tasks are identical to those in the preferred-direction experiment except that the optic-flow stimuli are stationary in the world in this experiment. Gaze tracking almost always occurred along the VORC preferred-null axis with small differences occurring if the pursuit and VORC preferred-null axes differed; we split the difference. Gaze rotations were performed in both the preferred and the null directions. The fixed gaze task was identical to the gaze tracking tasks except that the eye, head, and body were stationary in the room. The simulated gaze-rotation condition was identical to the fixed gaze condition except that the visual stimulus drifted in the direction opposite to the direction tracked in the gaze tracking tasks. This created a retinal stimulus identical to the retinal stimuli in the gaze-tracking tasks to the extent that eye movements were performed perfectly. Counter drifting the visual stimulus approximates counter rotating the visual stimulus quite well for the small, centrally located stimuli used in these experiments. Gaze trajectories were centered on the same room location across all tasks to equalize all gaze angles on average. Gaze rotated by ±4.6° ($\sqrt{2}$ more for diagonal gaze rotations) about the central location during the 1.0-s data-analysis period. The gaze trajectory center was located within 7.07° of the screen center, and the visual stimuli were centered within 14.1° of the gaze trajectory center. Gaze and stimulus centers were offset to position the optic-flow stimuli in the RF ''hot spot.''

Data analysis

Horizontal and vertical eye positions were sampled every millisecond and yaw and pitch head positions were sampled every 8 ms. Action potential event times were stored for off-line analysis with microsecond resolution. Neurons from two monkeys were recorded. Data trends are similar and significant in both monkeys so the data were pooled for analysis.

We analyzed the *preferred-optic-flow experiment* data with a nonparametric, one-way ANOVA (Kruskal-Wallis) to test for optic-flow pattern tuning. Each of the six locations was considered separately. Mean firing rates from three (*DAL*) or four (*FTZ*) replicates during the last 1.0 s of the 1.2-s stimulus presentation were used for the ANOVA.

We analyzed the *preferred-direction experiment* data to determine the preferred pursuit and VORC directions. We estimated these directions as the angle of the response-weighted vector sum (Fisher 1993; Geesaman and Andersen 1996). The preferred direction (ϕ) is equal to arctan(S/C), where S is the sum of $F_i \sin \phi_i$ and C is the sum of $F_i \cos \phi_i$ over all eight gaze-rotation directions ($i = 1, 2, \ldots, 8$). F_i and ϕ_i correspond to the average firing rate and specified gaze-rotation angle, respectively, associated with each of the eight gaze-rotation directions. The preferred direction was adjusted to the proper quadrant based on the signs of S and C. We also calculated the trigonometric mean which we used as a selectivity index (SI). SI is equal to $\sqrt{S^2 + C^2}$ divided by the sum of F_i over all eight gaze-rotation directions. Unlike other selectivity measures, such as 1 − (null/pref), which only indicate the modulation along a single axis, SI reaches unity (perfect selectivity) only if all nonpreferred directions are totally suppressed. An SI of zero indicates the complete lack of tuning.

Circular, nonparametric statistics were used to assess preferred-direction biases (Rayleigh) and cell-by-cell preferred-direction correlation (angular-angular correlation). We determined the significance of SIs with boot-strap methods: we created directional tuning curves by drawing (without replacement) eight mean firing rates from a given cell's response database, we randomly assigned the firing rates to the eight directions, and finally calculated the SI for this tuning curve. We repeated this procedure 1,000 times for pursuit and VORC for all cells. If the measured SI exceeded the 95% point of the simulated distribution, we considered the SI significant. We found that the Rayleigh test, which has been used previously for determining SI significance (Geesaman and Andersen 1996), is overly conservative. Finally a nonparametric correlation test (Spearman) was used to test for relationships between SIs in the population. All analyses used the mean firing rates from two (*FTZ*) or three (*DAL*) replicates during the last 1.0 s of the 1.2-s stimulus presentation.

We analyzed the *heading experiment* data to determine the influence of gaze tracking on the visual response. We constructed seven focus tuning curves for each neuron, one for each gaze tracking condition in both tracking directions, using mean firing rates and variances from three (*DAL*) or four (*FTZ*) replicates during the last 1.0 s of the 1.2-s stimulus presentation. We used Kruskal-Wallis analyses to assess the tuning significance for each focus tuning curve.

To understand the effects of preferred- and null-direction VORC, pursuit, and simulated gaze rotation, it is necessary to compare tuning curves in the different gaze-rotation conditions with the fixed-gaze condition tuning curve. In general, we found that gaze rotations preserved the primary shapes of the fixed-gaze tuning curves, which are often sigmoidal or Gaussian (examples will be presented in RESULTS). This observation led to our approach for comparing tuning curves: the relationship between two tuning curves with similar shapes can be characterized approximately by two parameters, one reflecting horizontal effects and one reflecting vertical effects.

Figure 4 shows three possible alignments of two focus tuning curves. Figure 4*A* illustrates a horizontal, or independent variable, offset between two tuning curves with related structures. We calculated this offset with a cross-correlation analysis, which provides a measure of tuning curve alignment at each relative horizontal offset, as one curve is shifted past the other. The optimal shift is identified as the relative horizontal offset with the maximum correlation coefficient. Parameterizing the vertical, or dependent variable, relationship is more difficult because the tuning curves are not necessarily functions (single valued) of the dependent variable, ruling out cross-correlation techniques. Moreover, as shown in Fig. 4*B*, the relationship between the curves may be described as multiplicative, additive, linear, or even nonlinear. Distinguishing between these possibilities has inherent difficulties and is beyond the scope of this report. Instead, we attempted to quantify the vertical relationship with a single parameter to describe the basic effect and to compare this effect across conditions. We compared multiplicative and additive measures and found that the χ^2 goodness-of-fit values were comparable across gaze-rotation conditions and across the population of cells. We chose the multiplicative measure for two reasons: multiplicative gain, or the ratio between two responses, is normalized automatically for firing rate so comparison between conditions and cells is straighforward and multiplicative gain commonly is used for characterizing modulatory effects (Brotchie et al. 1995; Snyder et al. 1998). To calculate the

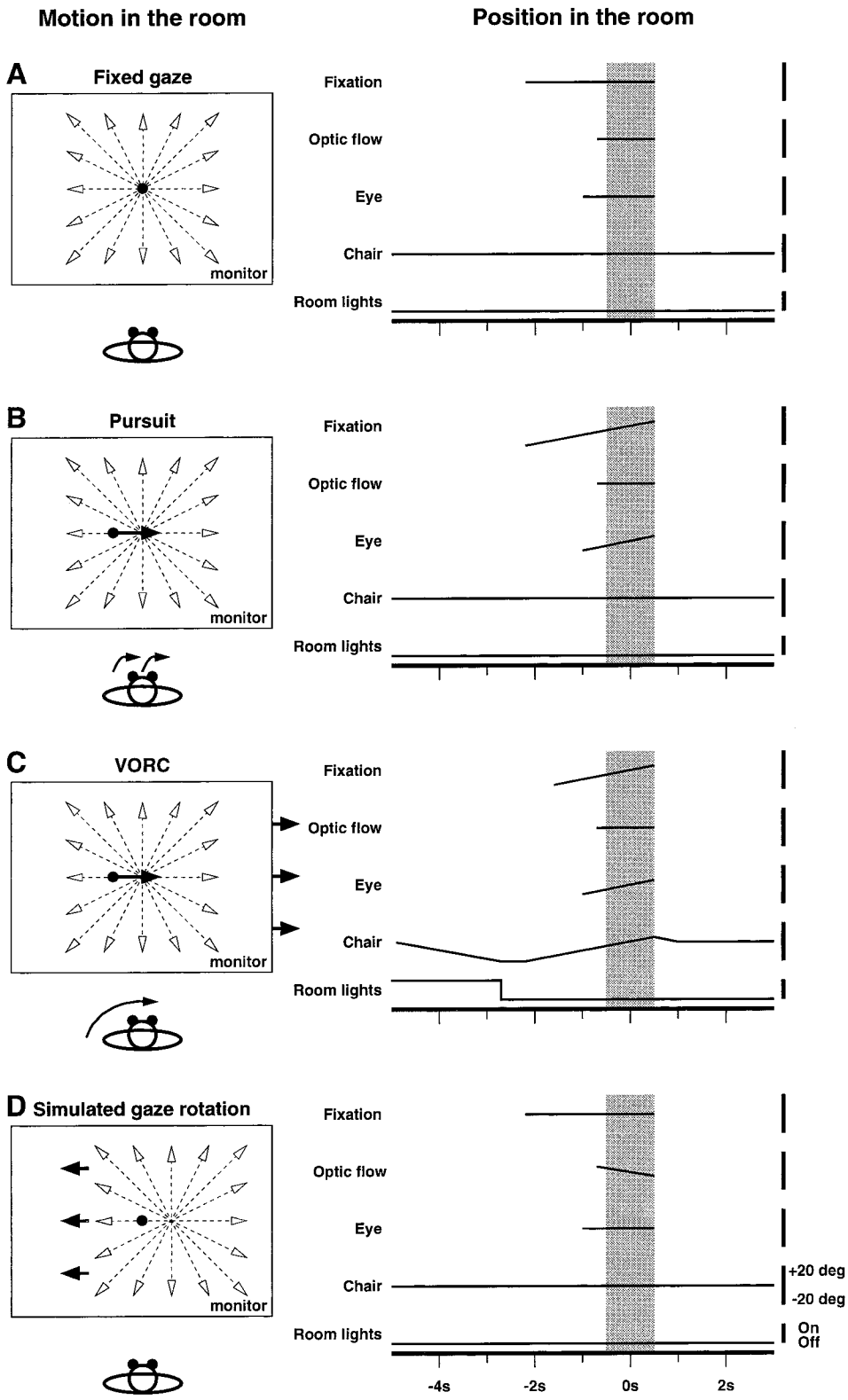

FIG. 3. Schematic illustrations and timing diagrams for the 4 behavioral tasks in the heading experiment. Rightward gaze rotation conditions are shown in this example, although gaze rotations were performed in the preferred and null directions in the experiment. *Left*: all arrows refer to movement in the room and indicate conditions during the data collection interval. *A*: fixed gaze task requires fixating a stationary target (solid circle) while viewing optic flow stimuli (dashed motion vector arrows). *B*: pursuit task requires pursuing a moving target (filled circle with filled arrow) while viewing optic-flow stimuli. *C*: VORC task requires fixating a target moving in register with the head and body (filled circle with filled arrow) while viewing optic-flow stimuli. Optic-flow stimulus location does not move in the room. *D*: simulated gaze rotation task requires fixating a stationary target while viewing optic-flow stimuli being counter drifted across the screen (stimulus movement indicated by 3 solid leftward arrows). Nine focus positions within the stimulus frame were presented to simulate a span of headings (an expansion pattern with a heading of 0° is shown here). Stimulus remains fixed in the world (*A–C*) or is drifted in the world (*D*). *Right*: timing diagrams plot the experimental conditions and behavioral requirements as a function of time. Lines represent physical positions in the room, hence parallel lines indicate no relative movement (only horizontal and yaw positions are shown for simplicity). Presence of a line indicates the presence of a stimulus (fixation and optic flow) or a positional requirement being enforced (eye and vestibular chair). For room lights, line position indicates the light status. Times are aligned to the middle (0.0 s) of the 1.0-s data-analysis period, shown in gray. Gaze rotated by ±4.6° about the central location during the 1.0-s data-analysis period. Onset times are as follows: −700 ms, optic-flow stimulus; −1.0 s, proper eye position required; and −2.2 s, fixation target appears. For VORC trials, onset times are as follows: −700 ms, optic-flow stimulus; −1.0 s, proper eye position required; −1.6 s, fixation target appears; and −2.2 s, chair begins sweep. At −2.7 s, the chair arrives at the ready position and the room lights are extinguished.

gain, we used the mean discharge rates during visual stimulus presentation as opposed to the difference between the peristimulus and the prestimulus discharge rates. Such subtraction would remove the additive contributions of the gaze-rotation signals, which is an influence we wish to consider.

Figure 4*C* illustrates the general case of two tuning curves related by a horizontal shift and a vertical gain. We adopted the following approach to characterize such a relation: *1*) calculate the optimal horizontal shift between the two curves by cross-correlation, which is insensitive to vertical gain and offset; *2*) subtract the optimal shift thereby horizontally aligning the curves; and *3*) calculate the gain over the range of tuning curve overlap. The effect of a given gaze-rotation condition thereby is characterized by two scalars, optimal shift and gain, and relates the gaze-rotation tuning curve to the fixed-gaze tuning curve.

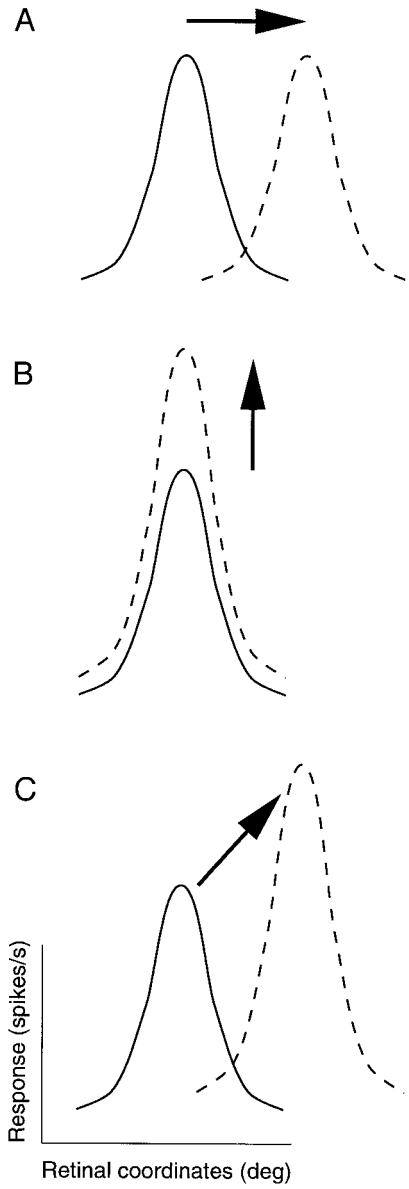

FIG. 4. Three possible alignments of 2 focus tuning curves. —, hypothetical fixed-gaze tuning curve; - - -, hypothetical gaze-rotation tuning curve. *A*: horizontal, or independent variable, offset between 2 tuning curves with similar structures. *B*: vertical, or dependent variable, changes in tuning curves caused by modulatory cues often are approximated as multiplicative. *C*: general case of 2 tuning curves related by both a horizontal shift and a vertical gain. These curves are related by the combined horizontal offset shown in *A* and the vertical gain shown in *B*.

Although cross-correlation has advantages and disadvantages compared with other methods, we adopted this method because the advantages are well suited for the specific questions we ask. Cross-correlation reduces to correlation at a given horizontal shift, as expressed

$$r_c(x, y) = \frac{\sum_{i=1}^{n} (x_i - \bar{x})(y_i - \bar{y})}{\sqrt{\sum_{i=1}^{n} (x_i - \bar{x})^2 \sum_{i=1}^{n} (y_i - \bar{y})^2}} \quad (2)$$

The mean response vectors for the two tuning curves are x and y, and $\bar{x}$ and $\bar{y}$ are the average responses of the two tuning curves.

Cross-correlation is well suited to our analysis approach for several reasons. First, it is quite sensitive to the tracking, or alignment, of two tuning curves regardless of the exact functional form of the curves. This allows us to avoid curve fitting (e.g., sigmoids or Gaussians), which would be appropriate for only a part of the data given the strict assumptions of parametric methods. Second, cross-correlation is insensitive to vertical shifts between the two tuning curves, which is apparent in the correlation equation by substituting $x + k$ for y, where k is a scalar vertical offset: this case reduces to autocorrelation (independent of k). Finally, cross-correlation is insensitive to vertical, multiplicative gains between two tuning curves and is apparent in the correlation equation by substituting gx for y, where g is a multiplicative gain: this case also reduces to autocorrelation (independent of g).

However, we also must contend with two limitations. First, we restricted the total range of shifts tested so as to avoid situations where fewer than five data points overlap. We found that less than five overlapping points results in erroneously high correlation values due to alignment of the edges of the tuning curves not to the alignment of the prominent features of the tuning curves that we sought. This shift range is -8 to $+56°$, where 0° corresponds to retinal coordinates and 24° corresponds to screen coordinates. Screen coordinates, or equivalently room coordinates, is an operational term and alignment in screen coordinates indicates complete compensation for gaze rotation (Bradley et al. 1996). Alignment in retinal coordinates indicates no compensation for the visual effects of gaze rotation. Second, if the prominent features (e.g., minima, maxima, inflection points) of two tuning curves are aligned, but the shape of one or both of the two tuning curves is altered slightly, this can lead to misestimations of the alignment of the prominent features. However, this misestimation grows as the extent of the shape change increases, which means that the misestimation is small for small shape changes. Alternate methods also suffer from such misestimations, but cross-correlation deviates from what we consider proper alignment of prominent features in a graded manner.

We began the cross-correlation analysis by smoothing the tuning curves with a three-point moving average (twice; uniform weights) followed by a spline interpolation (1° sampling). Although all results are qualitatively similar without smoothing and interpolation, such methods provide reasonable intersample interpolation and reduce anomalous cross-correlogram peaks at the edges of the correlation range. Cross-correlation results also remained qualitatively similar for tuning curves formed by integrating activity as brief as 200 ms, centered on the midpoint of the data collection interval.

Nonparametric tests were used to analyze cross-correlation population data. Wilcoxon *t*-tests were used to determine the significance of optimal shifts in the various gaze tracking tasks across the population. Mann-Whitney *t*-tests were used to test if distribution means are different. Spearman correlation tests were used to determine if a significant correlation exists between optimal shifts in different gaze tracking conditions across the population. Nonparametric tests also were used to evaluate gain data.

Gaze tracking conditions along diagonal axes result in tuning curves with focus spacings of $8\sqrt{2}$° instead of 8°. However, the theoretical shift along these axes also is expanded to $24\sqrt{2}$°. Because the focus spacing, theoretical shift, and tracking speeds all scale proportionally, the resulting shifts are readily remapped (i.e., divide shift by $\sqrt{2}$) for inclusion with the rest of the population data.

RESULTS

We recorded and analyzed data from 80 neurons in two monkeys, 56/80 from *monkey FTZ* and 24/80 from *monkey DAL*, in the preferred-optic-flow, preferred direction, and heading experiments.

Optic-flow tuning

We measured the response of MSTd neurons to expansion (EX), contraction (CO), clockwise rotation (CW), and counterclockwise rotation (CCW) optic-flow stimuli presented at six locations. We found most cells to be tuned significantly for the pattern of optic flow in at least one of the stimulus locations (54/80, 67.5%, $P < 0.05/6$, Kruskal-Wallis). Although additional trial replicates likely would increase the number of significantly tuned cells, we were able to identify clear tuning trends in all neurons. We conserved trials in this experiment, and in the preferred-direction experiment, because the heading experiment (the core experiment) required many long trials.

We noted the stimulus location eliciting the strongest tuning, and we refer to the preferred-optic-flow pattern at this location as the preferred-optic-flow pattern of the cell. The distribution of preferred-optic-flow patterns in the population is as follows: 43/80 (54%) EX, 24/80 (30%) CO, 9/80 (11%) CW, and 4/80 (5%) CCW. We also noted the preferred-optic-flow pattern at the location centered on fixation, which was typically the same as the cell's preferred-optic-flow pattern, for use in the preferred-direction experiment.

Although large optic-flow patterns elicit the strongest neural responses, we were restricted to 18 × 18° visual stimuli. However, we routinely found strong, tuned responses that were modulated by the position of the stimulus within the receptive field. These characteristics are indicative of well-activated MSTd neurons. We also found similar proportions of cells selective for expansion, contraction, and rotation (54, 30, and 16%, respectively) as compared with our previous study in a different monkey (41, 33, and 27%, respectively) which used 50 × 50° stimuli (Bradley et al. 1996). These similarities indicate that MSTd response characteristics persist as stimulus size decreases and are consistent with a previous report (Graziano et al. 1994).

Pursuit and VORC tuning

We then recorded neural activity during the preferred-direction experiment and analyzed the responses to determine the preferred-pursuit and preferred-VORC directions. Figure 5*A* shows the basic result that individual MSTd neurons are tuned for the direction of both pursuit and VORC. The response of this neuron clearly is enhanced during rightward (ipsilateral) pursuit and VORC and clearly is suppressed during leftward (contralateral) pursuit and VORC. The estimated preferred pursuit and VORC directions are 0.7 and 344.8° (−15.2°), respectively (angle of the response-weighted vector sum). Angles are measured counter clockwise from the ipsilateral direction. The preferred gaze-rotation directions are well aligned in this cell (15.9° difference), considering that the possible range of direction differences is 180°. The directions opposite the preferred directions are designated the null directions and also were noted for use in the heading experiment.

To visualize the degree of directional tuning in the population, Fig. 5*B* plots tuning curves averaged across the population. Pursuit and VORC tuning curves from each neuron were rotated (independently) to align preferred directions at 0°. The curves were normalized (separately) to the preferred-direction responses before averaging across the population. Mean pursuit and VORC tuning curve shapes are quite similar, indicating similar directional selectivities in the population. Pursuit has a slightly sharper mean tuning curve, but both pursuit and VORC have preferred:null response ratios of ~2:1 and both have tuning bandwidths (full width at half-maximum) of ~90°.

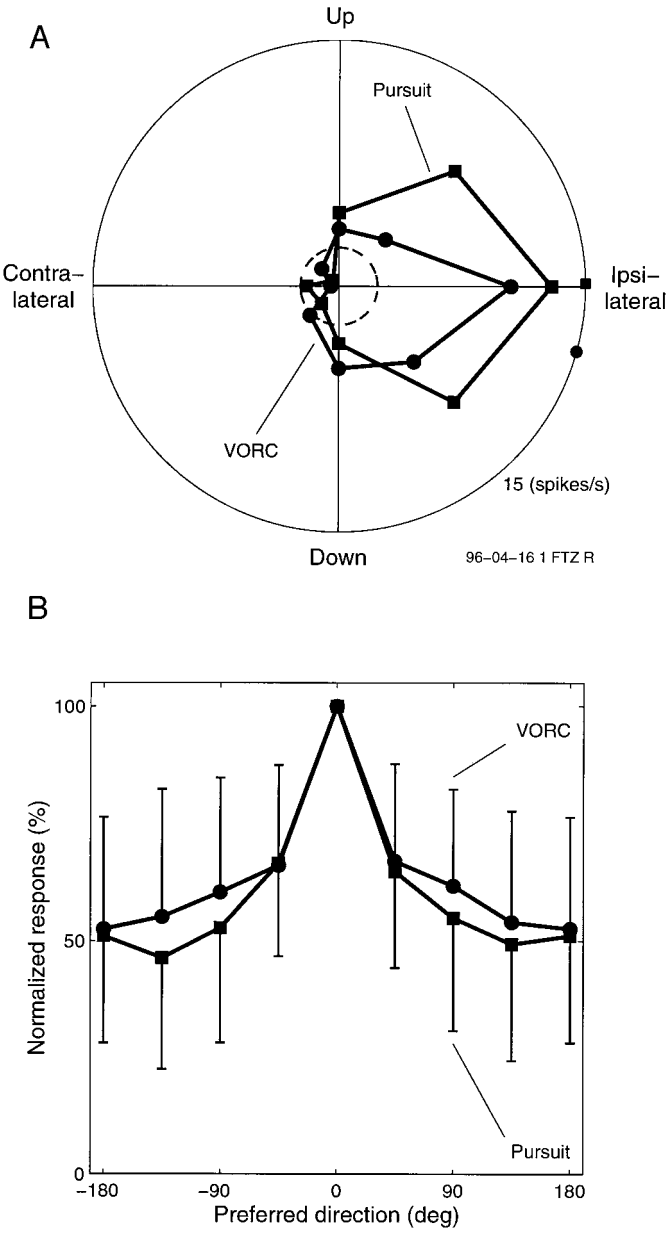

FIG. 5. Gaze-tracking activity in the preferred-direction experiment. *A*: response of a neuron during pursuit (■) and VORC (●), in each of 8 directions. Data points are the mean firing rate of 2 replicates. - - -, spontaneous discharge rate of 2.4 spikes/s. Spontaneous discharge rate is the mean activity during the 500 ms preceding optic-flow presentation in the preferred-optic-flow experiment (96 repetitions). Preferred directions for pursuit and VORC are indicated by ■ and ●, respectively, located along the plot perimeter. Pursuit direction selectivity index (SI) is 0.527 and the VORC SI is 0.445; both are significant ($P < 0.05$, boot-strap). *B*: average response of all neurons ($n = 80$) as a function of gaze-rotation direction relative to the preferred directions. Pursuit and VORC preferred directions were selected as the measured directions with maximum response and were rotated (separately), along with the entire tuning curves, to 0°. All tuning curves were normalized to the preferred-direction firing rate (100%) before averaging across the population. ■, pursuit conditions (−1 SD error bar); ●, VORC conditions (+1 SD error bar).

Does this similarity between pursuit and VORC tuning, seen

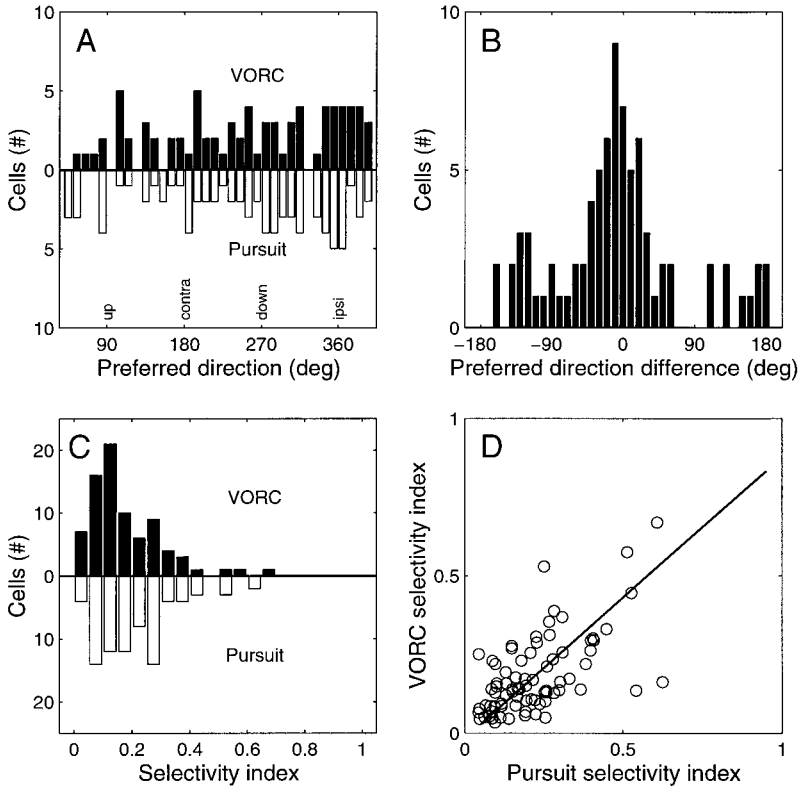

FIG. 6. Comparison of pursuit and VORC preferred directions and directional selectivity in the preferred-direction experiment. *A*: population histograms of the preferred directions for pursuit, plotted as downward bars, and VORC, plotted as upward filled bars. Histogram binwidth is 10°, and we broke the circular geometry at 40° for plotting purposes. *B*: population histogram of the cell-by-cell difference between the VORC- and pursuit-preferred directions. Positive differences were selected arbitrarily to indicate VORC-preferred directions counterclockwise relative to pursuit-preferred directions. Histogram binwidth is 10°. *C*: population histogram of the selectivity indices for pursuit, plotted as downward bars, and VORC, plotted as upward filled bars. Histogram binwidth is 0.05. VORC and pursuit distributions have 25th, 50th, and 75th percentile points of 0.09, 0.14, and 0.24 and 0.11, 0.19, 0.27, respectively. *D*: correlation plot of VORC against pursuit selectivity indices and best-fit line.

in the population, arise from an equivalence at the single-cell level? To answer this question, we examined the distribution of preferred directions, the cell-by-cell difference in preferred directions and the cell-by-cell preferred-direction correlation, the population distribution of directional selectivity indices, and the cell-by-cell correlation of these indices.

Figure 6*A* shows population histograms of the pursuit and VORC preferred directions. Both distributions appear to favor some directions over others. The downward-ipsilateral direction is favored significantly for pursuit ($P < 0.01$, Rayleigh) and although VORC failed to reach significance ($P = 0.31$, Rayleigh), there appears to be a similar trend. Figure 6*B* is a population histogram of the cell-by-cell difference between the VORC and pursuit preferred directions. A single, strong peak occurs at ~0° (−7.7 ± 80.1°, mean ± SD) and is significant ($P < 0.001$, Rayleigh). The preferred directions also are correlated significantly on a cell-by-cell basis ($r_{aa} = 0.08$, $P < 0.01$, nonparametric angular-angular correlation). These findings indicate that individual cells tend to have well-aligned pursuit and VORC preferred directions.

We quantified the pursuit and VORC directional tuning in each cell with a selectivity index (SI). Figure 6*C* plots population histograms of the SIs. Both populations are quite selective with pursuit slightly more selective on average. We found that 20/80 (25%) cells have significant pursuit tuning and 16/80 (20%) cells have significant VORC tuning ($P < 0.05$, bootstrap analysis of SIs). As with optic-flow pattern tuning, these percentages are likely underestimates due to the relatively low number of repetitions. Nevertheless, as Fig. 5*B* shows quite directly, there is clear evidence that pursuit and VORC signals are well tuned and we were able to identify clear tuning trends in all neurons.

Figure 6*D* plots VORC SIs versus pursuit SIs on a cell-by-cell basis. We found a significant correlation in these data ($P < 0.001$, $r_s = 0.58$, Spearman) and the best fit line has a slope of 0.89 (2-dimensional least mean squares fit). This indicates that pursuit and VORC directional selectivity is related, and is nearly equal, in individual neurons.

With evidence that pursuit and VORC gaze-tracking signals are similarly tuned in individual neurons, we now examine how these gaze-tracking signals interact with visual-motion patterns simulating translation through the world (i.e., heading experiment).

Focus tuning

The heading experiment consists of fixed gaze, pursuit, VORC, and simulated gaze-rotation conditions conducted along the cell's preferred-null axis. Figure 7 presents all neural and behavioral data collected from a single MSTd neuron in the heading experiment. The seven rows represent the seven behavioral/directional combinations while the nine columns represent the FOE positions on the screen. Comparisons of the relative alignment and magnitude of the various behavioral/directional tuning curves are presented in the following two sections, SHIFT COMPENSATION and GAIN MODULATION.

The fixed-gaze response (Fig. 7, *middle*) is a typical example of how the neural response changes as the focus position is varied along the cell's preferred-null gaze-rotation axis (Fig. 7, schematic illustrations). The preferred-optic-flow pattern for this cell is expansion and the preferred gaze-rotation direction is rightward. The fixed-gaze response is tuned for the FOE position ($P < 0.001$, Kruskal-Wallis), responding vigorously to leftward FOE positions but hardly at all to rightward FOE positions. Although this neuron was classified as expansion selective, because it responded better to expansion patterns

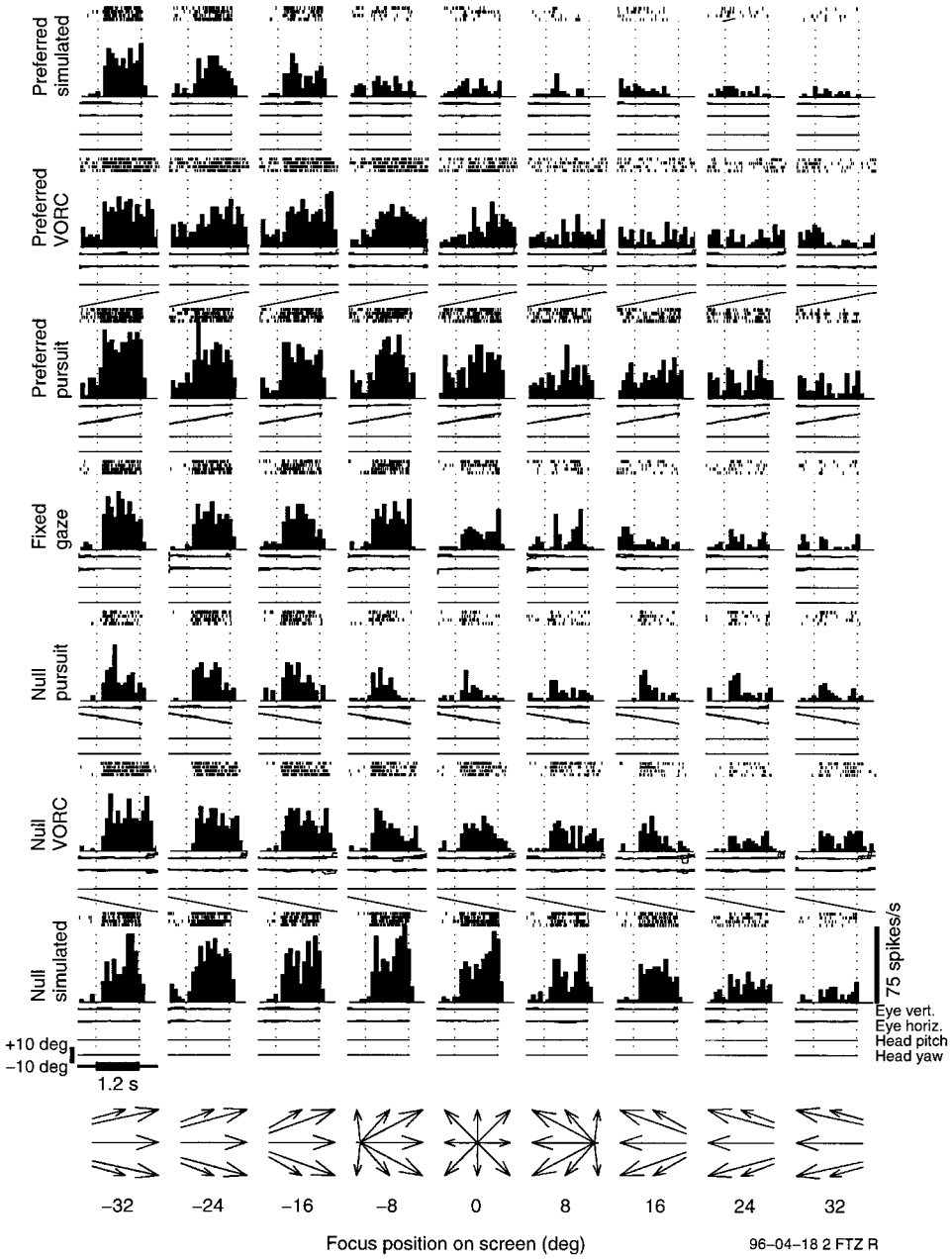

FIG. 7. Neural and behavioral data collected from a single MSTd neuron in the heading experiment. *Rows*: seven behavioral/directional combinations; *columns*: FOE positions on the screen. Preferred-direction conditions are grouped in the *top 3 rows* and null-direction conditions are grouped in the *bottom 3 rows.* Optic-flow illustrations are drawn at one-third scale, referenced to the abscissa scale, and the FOE is beyond the stimulus frame for all but the central 3 FOE positions. Action potential raster plots (4 repetitions), action potential peristimulus time histograms (PSTHs; 100-ms time bins), horizontal and vertical eye position traces (1-ms sample period, + indicates right or up), and yaw and pitch head position traces (8-ms sample period, + indicates yaw right or pitch up) are shown for each condition. The 1.2-s stimulus period (thick bar on time scale) is indicated by vertical dotted lines, and the last 1.0 s of this period was analyzed to construct focus tuning curves for each of the seven behavioral/directional conditions. The 500-ms periods before and after the visual stimulus are indicated by thin bars on the time scale. This neuron is selective for expansion patterns and the preferred gaze-rotation direction is rightward. Tuning curves for this cell are shown in Fig. 8.

than to contraction or rotation patterns, it also responds to nearly laminar motion. This is evident in the fixed-gaze response because the −32° FOE stimulus (nearly rightward laminar flow) elicits a strong response. That FOE tuning arises from the combination of expansion (or contraction or rotation) and laminar motion selectivities is not surprising. Moreover by varying the FOE positions along the preferred-null gaze-rotation axis, we expect to couple into the neuron's laminar flow response because it has been reported that most MSTd neurons have laminar motion selectivities that align with the preferred-null pursuit axis (Komatsu and Wurtz 1988b).

The fixed-gaze response appears to reliably encode the FOE position, but does it represent the FOE position on the retinae or the FOE position on the screen (in the world)? Retinal and screen coordinates are identical when the gaze is fixed. To dissociate retinal FOE position tuning from true heading tuning, which requires the cell to encode the FOE position on the screen, we must consider the neuron's focus tuning while gaze is rotating because the retinal focus is shifted then relative to the screen (see Fig. 1). Constant-velocity pursuit, VORC, and simulated gaze rotations introduce a constant FOE position difference, or displacement, between the retinal and screen images. Cell-by-cell comparisons of pursuit, VORC, and simulated gaze-rotation focus tuning curves with the fixed gaze focus tuning curve are discussed below.

To verify that MSTd neurons are sensitive to the dimension of visual motion that we varied, we tested the significance of FOE position tuning for each behavioral/directional tuning curve. The number of neurons in the population with significant tuning is as follows: 53/80 (66%) fixed gaze; 34/80 (43%) preferred-direction VORC; 40/80 (50%) null-direction VORC; 45/80 (56%) preferred-direction pursuit; 34/80 (43%) null-

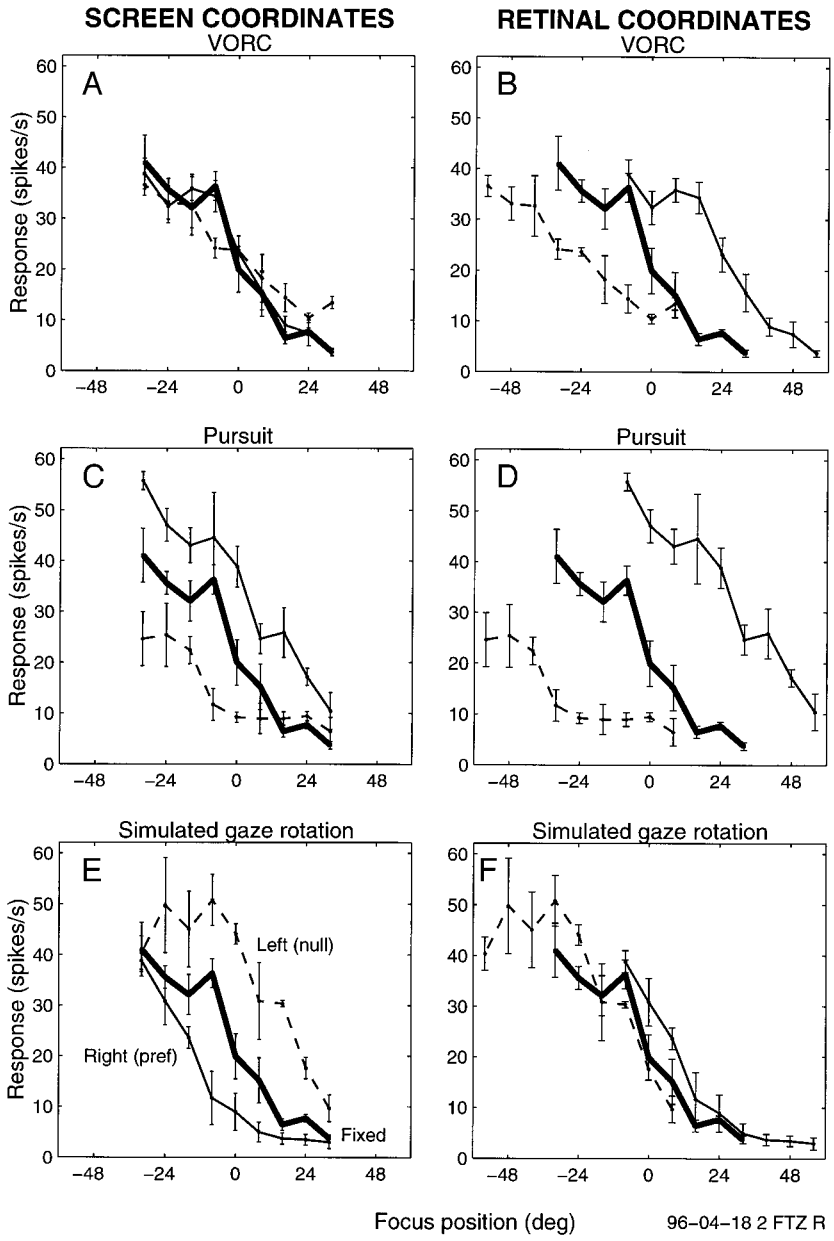

FIG. 8. Response of a single ''heading'' neuron in the heading experiment. Focus tuning curves from the 3 gaze rotation conditions (*rows*) are plotted in the coordinates of the screen (*left*) and the retinae (*right*). Fixed gaze curve (thick solid line) is identical in all panels. Preferred (solid lines) and null (dashed lines) tuning curves are displaced by the theoretical shift offsets of +24 and −24°, respectively, with respect to the fixed gaze curve to plot the curves in retinal coordinates. Data points are means ± SE for 4 replicates (see Fig. 7 for rasters, PSTHs, eye traces, and head traces).

direction pursuit; 45/80 (56%) preferred-direction simulated gaze rotation; and 45/80 (56%) null-direction simulated gaze rotation ($P < 0.05$, Kruskal-Wallis). We expected to find fewer significantly tuned cells in the gaze-rotation conditions than in the fixed gaze condition because gaze rotation adds laminar flow to the retinal image, thereby causing more stimuli to have essentially laminar retinal flow. Neurons respond more similarly to visual patterns with only slight variations from laminar flow than to visual patterns that span both directions of laminar flow and, for example, expansion (see Fig. 7). Few cells are tuned significantly for focus position in all seven behavioral/directional conditions (12/80, 15%, $P < 0.05$, Kruskal-Wallis), but most cells are for at least one of the seven conditions (59/80, 74%, $P < 0.05/7$, Kruskal-Wallis).

Influence of gaze rotation

SHIFT COMPENSATION. Figure 8 plots tuning curves constructed from the heading experiment data presented in Fig. 7. Rows represent the three gaze-tracking conditions, which are retinally identical except for the visual effects caused by extremely small eye-movement deviations during fixation, pursuit, and VORC. The curves are plotted in both the coordinates of the screen and the retinae to help visualize the alignment of features.

Tuning curve minima, maxima, and inflection points appear to align better in screen coordinates than in retinal coordinates for VORC and pursuit conditions. Vertical differences between tuning curves are discussed later in the paper. Neurons with pursuit and VORC tuning curves that align in screen coordinates, which represent the coordinates of the environment, are termed ''heading cells'' because they appear to encode heading regardless of eye or head rotations. The observation that relative response properties, such as minima and maxima, often appear not to shift horizontally even in the face of large

changes in the retinal image raises the possibility that heading may be encoded as relative firing rates as opposed to absolute firing rates. For some conditions in a few neurons, Fig. 8*A* for example, even the absolute firing rates are essentially invariant to the altered retinal images.

The neuron in Fig. 8 clearly does not simply report the pattern of visual motion falling on the retinae. Instead this neuron is able to use either the extraretinal signals or the rotational movement of the visual stimulus to align the tuning curves better in screen coordinates than in retinal coordinates. To determine which of these possibilities is responsible for the tuning curve shifts, or compensation, we consider the simulated gaze-rotation conditions. The preferred- and null-direction simulated gaze-rotation conditions are retinally identical to the preferred- and null-direction pursuit and VORC conditions, respectively, to the extent that pursuit and VORC are identical to fixation. Any difference in response properties must be due to the pursuit or VORC signals present during real gaze rotation. The simulated gaze-rotation tuning curves from the neuron shown in Fig. 8 appear to align better in retinal coordinates than in screen coordinates. Figure 8*F* shows that the tuning curves align to form a single, extended tuning curve in retinal coordinates. This neuron simply reports the pattern of visual motion on the retinae when no extraretinal signals are present. This observation suggests that pursuit and VORC signals contribute to the compensation mechanism responsible for aligning tuning curves in screen coordinates.

To quantify the alignment of relative response features, we cross-correlated preferred- and null-direction tuning curves (separately) with the fixed gaze tuning curve for each gaze-rotation condition. We measured optimal alignments with respect to retinal coordinates: 0° shift indicates alignment in retinal coordinates, 24° shift indicates alignment in screen coordinates, and intermediate shifts indicate alignment in between. Positive shifts are in the direction theoretically required to bring the tuning curves into alignment for representing heading in the world, and therefore we term positive shifts ''compensatory shifts'' because they tend to compensate for the effects of gaze rotation.

Figure 9*A* plots the population average cross-correlograms for VORC, pursuit, and simulated conditions. Preferred- and null-direction cross-correlograms are similar and are pooled in this graph. The population average cross-correlogram for the simulated condition peaks closer to 0° (less compensation) than does the pursuit cross-correlogram. The VORC cross-correlogram also peaks to the right (greater compensation) of the simulated peak, although this is difficult to see in the population average cross-correlograms.

To more clearly see the behavior of single cells, we must identify the optimal simulated, pursuit and VORC shift for each cell. Figure 9*B* plots population histograms of the optimal compensatory shifts for the three gaze-rotation conditions. A cell's optimal shift in a given condition is the shift that produces the maximum correlation value. Preferred- and null-direction shifts are pooled because both directions compensate similarly. Table 1 contains the 25, 50, and 75% percentile points for all pooled, preferred, and null distributions as well as results from all shift analyses. All three distributions show a pronounced peak at ~8°, which is partly due to the 8° binwidth, and actually have a relative peak arrangement consistent with that in Fig. 9*A*. Compared with the simulated gaze-

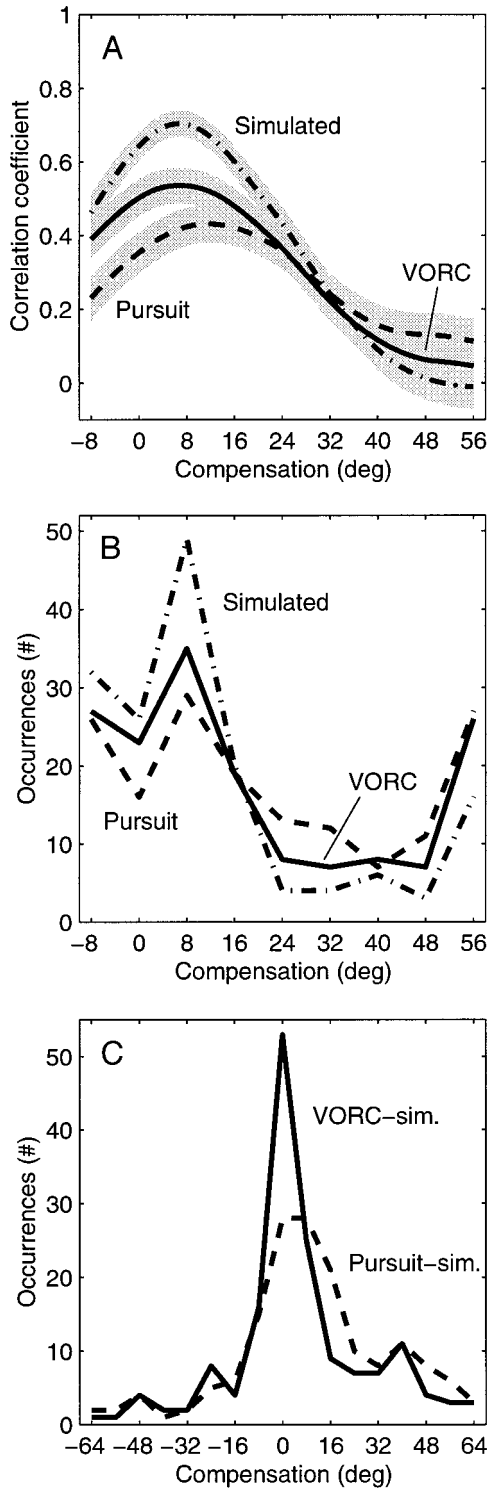

FIG. 9. Population cross-correlograms and histograms of compensatory shifts for the 3 gaze-rotation conditions. In all panels, preferred- and null-direction data are pooled. *A*: population average cross-correlograms for VORC (solid curve), pursuit (dashed curve), and simulated (dot-dashed curve) conditions. Gray bands represent the ±1 SE range. *B*: population histograms of VORC, pursuit, and simulated compensatory shifts (line styles as in *A*). Binwidth is 8.0°. Table 1 lists all distribution parameters and hypothesis test values. *C*: population histograms of VORC shifts minus simulated shifts (solid curve) and pursuit shifts minus simulated shifts (dashed curve). Binwidth is 8.0°. Subtraction was performed on a cell-by-cell basis, and Table 1 contains all distribution and test values.

TABLE 1. *Compensatory shift-related distribution parameters and significance values*

Distribution	Related Figure	25th Percentile, °	Median, °	75th Percentile, °	Wilcoxon, T	Spearman, r_s	Significance	Mean, °	Compensation, %
Histograms									
Pooled VORC	9*B*	2.0	12.0	37.5	1,279	—	$P < 0.001$	18.5	77.2
Pooled pursuit	9*B*	3.5	15.5	41.0	1,099	—	$P < 0.001$	21.2	88.4
Pooled simulated	9*B*	−0.5	7.5	15.5	2,090	—	$P < 0.001$	12.5	52.0
Preferred VORC	—	1.0	11.0	42.0	350	—	$P < 0.001$	19.4	80.6
Null VORC	—	4.0	12.0	32.5	300	—	$P < 0.001$	17.7	73.8
Preferred pursuit	—	0.5	11.5	37.0	400	—	$P < 0.001$	18.4	76.6
Null pursuit	—	6.5	19.0	49.5	180	—	$P < 0.001$	24.0	100.1
Preferred simulated	—	0.5	7.0	15.0	539	—	$P < 0.001$	11.5	47.8
Null simulated	—	−2.0	8.0	19.5	514	—	$P < 0.001$	13.5	56.2
Pooled VORC − simulated	9*C*	−3.0	2.0	15.5	3,151	—	$P < 0.001$	6.1	25.3
Pooled pursuit − simulated	9*C*	−3.5	7.0	23.5	2,696	—	$P < 0.001$	8.7	36.4
Preferred VORC − simulated	—	−3.0	4.0	19.0	784	—	$P < 0.001$	7.9	32.9
Null VORC − simulated	—	−3.0	1.5	12.0	796	—	$P < 0.001$	4.2	17.6
Preferred pursuit − simulated	—	−4.0	7.5	20.5	715	—	$P < 0.001$	6.9	28.9
Null pursuit − simulated	—	−3.5	4.5	27.0	648	—	$P < 0.001$	10.5	43.9
Correlations									
Preferred vs. null VORC	—	—	—	—	—	0.197	$P > 0.05$	—	—
Preferred vs. null pursuit	—	—	—	—	—	0.211	$P > 0.05$	—	—
Preferred vs. null simulated	—	—	—	—	—	0.249	$P < 0.05$	—	—
Pooled VORC vs. pursuit	10*A*	—	—	—	—	0.356	$P < 0.001$	—	—

A description of the distribution and the related figure, if any, are listed on rows along with distribution parameters (25%, median, 75%, and mean values) and hypothesis test values (Wilcoxon *t*-test and Spearman rank correlation). Significance values refer to either Wilcoxon or Spearman tests with null hypotheses that the distributions are centered on zero or that no correlation is present, respectively. Compensation is defined as the ratio of the distribution mean (°) to the theoretical shift (24°) expressed as a percentage. Correlation tests do not apply to histograms (—) and distribution parameters and *t*-tests do not apply to correlation plots (—). VORC, vestibulo-ocular reflex cancellation.

rotation condition, the VORC and pursuit distributions have lower peaks in the 0° range and are fanned out in the compensatory (positive) direction. Because all distributions contain the same number of occurrences, with one cell contributing a preferred-direction occurrence and a null-direction occurrence, the areas under the curves are the same. Therefore, Fig. 9*B* shows that many MSTd neurons compensate, to a greater or a lesser extent, for the retinal effects of gaze rotation and many do not compensate at all.

Occurrences at the edges of the cross-correlation range likely have even more extreme optimal shifts, which could be detected with a wider range of focus positions. Such boundary effects are inherent to this class of analysis, which attempts to determine optimal alignments with a finite measurement range. The tendency for pursuit and VORC conditions to compensate more than the simulated condition is evident even in the boundary effect occurrences.

All three distributions are shifted significantly away from zero ($P < 0.001$, $n = 160$, Wilcoxon) but to different extents. The VORC and pursuit distribution means are significantly different from (larger than) the simulated distribution mean ($P < 0.01$ and $P < 0.001$, respectively, Mann-Whitney), but the VORC and pursuit distribution means are not significantly different from each other ($P = 0.328$, Mann-Whitney). The VORC, pursuit, and simulated gaze-rotation distributions have mean shifts of 18.53, 21.21, and 12.47°, respectively. When the means are expressed as the percent of complete compensation (24°), VORC, pursuit, and simulated gaze-rotations compensate by 77.2, 88.4, and 52.0%, respectively. These results show that the visual motion (rotational flow) present in the simulated gaze-rotation drives ~50% of complete compensation. When VORC or pursuit cues are also available, compensation rises beyond the 50% level reaching nearly 80 and 90%, respectively.

Does the increased compensation in the population during real-gaze rotations arise from most neurons compensating some or, alternatively, from only a few neurons compensating extensively? Figure 9*C* is a histogram of VORC shifts minus simulated shifts and pursuit shifts minus simulated shifts on a cell-by-cell basis. We again pooled data across preferred and null directions as the distributions are similar in both directions. These distributions reflect the portion of the total shift that is attributable to VORC or pursuit cues because the retinal contribution to each shift has been subtracted. If most MSTd neurons compensate some given retinal gaze-rotation cues but compensate even more when VORC or pursuit cues are also available, then we would expect the histograms in Fig. 9*C* to be skewed toward positive values and to have a single mode. This would presumably reflect a single population with a common compensation mechanism. On the other hand, if there is one group of neurons that compensates primarily with retinal gaze-rotation cues and another group that compensates primarily with VORC or pursuit cues, then we would expect the distribution to have two peaks, one at zero and one to the right of zero. Figure 9*C* shows that both the VORC and the pursuit distributions are skewed to the right with a primary peak around 0°. This is consistent with the single population hypothesis. Note that there is a small secondary peak in both distributions at ~40°, which may reflect a small group of neurons that compensate substantially during real gaze rotations but little during simulated rotations. It appears that most MSTd neurons compensate more given VORC or pursuit signals than given retinal signals alone, although we cannot rule out a second population of neurons that compensate extensively given pursuit or VORC cues.

We analyzed the distributions in Fig. 9*C* to quantify the previous observations. Both of these pooled distributions, as well as preferred- and null-direction distributions considered

separately, are skewed significantly toward positive values confirming that VORC and pursuit cues tend to drive greater levels of compensation in single neurons than do retinal signals alone ($P < 0.001$, Wilcoxon; see Table 1). The VORC-simulated and pursuit-simulated distributions have mean shifts of 6.1 and 8.7°, respectively, which translate to 25.3 and 36.4% of complete compensation. This evidence suggests that most individual MSTd neurons use a combination of retinal and VORC or pursuit cues to compensate at least partially for the retinal effects of gaze rotation.

To further investigate how MSTd neurons may represent heading, even while the direction of gaze rotates, we asked two additional questions. First, how do individual neurons compensate for preferred- and null-direction gaze rotations and, second, how do individual neurons compensate for VORC and pursuit gaze rotations? It is possible that MSTd neurons account for both the direction of gaze rotation and the type of gaze rotation.

To answer the first question, we correlated preferred-direction compensatory shifts versus null-direction compensatory shifts, on a cell-by-cell basis, in each of the three gaze-rotation conditions (e.g., preferred vs. null VORC shifts). There is not a significant correlation for either VORC or pursuit conditions ($P > 0.05$, Spearman), but there is a significant correlation for the simulated gaze rotation condition ($P < 0.05$, Spearman). Table 1 lists all correlation values. This indicates that most individual neurons are not able to compensate for both preferred- and null-direction VORC or pursuit. However, there are several neurons that do compensate for both preferred- and null-direction simulated gaze rotations. This suggests that the retinal-based component of compensation, which is present during simulated gaze rotation, is better able to compensate for two directions of rotation than is the pursuit or VORC based component of compensation. The importance of such directional equality being present or absent at the single neuron level is not clear because the output from two neurons, with opposite preferred directions, could effectively provide directionally invariant compensation.

The second question is how individual neurons compensate for VORC and pursuit gaze rotations. Figure 10*A* is a correlation plot of VORC versus pursuit shifts. Preferred and null directions are pooled in this plot, and all distribution parameters and test values are listed in Table 1. VORC and pursuit shifts are significantly correlated ($P < 0.001$, $r_s = 0.356$, Spearman), and the best fit line has a slope of 0.95 (2-dimensional least means square fit). There is a clear band of cells that fall along the unity diagonal and, therefore, compensate for VORC and pursuit gaze rotations approximately equally. The compensation magnitude ranges from −8° (*bottom left*) to +56° (*top right*). Cells with VORC and pursuit shifts of 24° perfectly compensate for the retinal effects of both types of gaze rotation, whereas cells with larger shifts overcompensate and cells with smaller shifts undercompensate. There are also two clusters of cells that primarily compensate only during VORC (*top left*) or during pursuit (*bottom right*). The clusters appear to be separated from the primary diagonal band of cells by two diagonal bands containing few or no cells. This plot and the correlation analysis suggest that most MSTd neurons use both VORC and pursuit signals to compensate the retinal effects of gaze rotation to similar extents.

Any categorization of occurrences, and therefore neurons, in Fig. 10*A* is essentially arbitrary because we understand neither how this cortical area is read out nor the dimensions along which heading information is encoded. Nevertheless, the data suggest a few boundaries, and we add an arbitrary division to

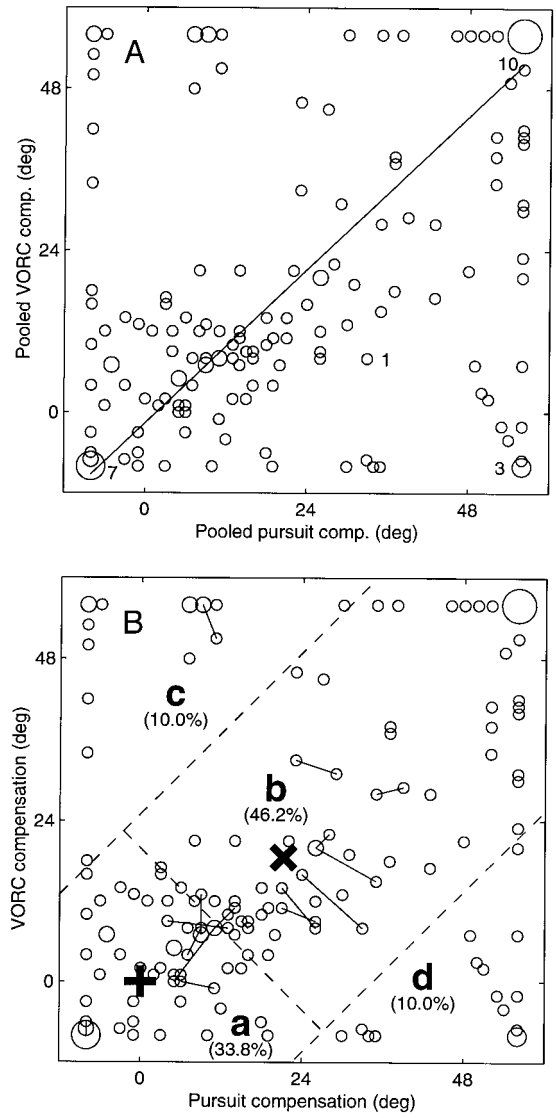

FIG. 10. Correlation plots of the compensatory shifts in individual neurons during VORC and pursuit gaze rotations. Preferred- and null-direction shifts are pooled in both panels. *A*: VORC vs. pursuit compensatory shift correlation plot. Area of ○ is proportional to the number of occurrences with that pair of shift values and 1, 3, 7, and 10 occurrences are labeled. *B*: correlation plot from *A* with 4 subpopulations delineated. Space of VORC compensation vs. pursuit compensation can be sectioned arbitrarily into 4 groups: neurons with little correlation and compensation (a), neurons with appreciable correlation and compensation (b), neurons with only appreciable VORC compensation (c), and neurons with only appreciable pursuit compensation (d). +, 0 compensatory shifts; ×, mean population shifts of 18.53° (18.53°/24° = 77.2% compensation) for VORC and 21.21° (21.21°/24° = 88.4% compensation) for pursuit. Boundary between regions a and b is midway between 0 and the mean shifts (- - -) and extends to 2 other boundary lines. Regions a and b, consequently, represent 33.8 and 46.2% of the population, respectively. Regions c and d each represent 10% of the population, by definition, farthest from the unity diagonal. - - - demarcating regions c and d are, consequently, 25.0 and 34.5° from the unity slope diagonal, respectively, and coincidentally fall within the underpopulated diagonal bands. Some cells have similar preferred- and null-direction pursuit and VORC shifts. Cells that have preferred- and null-direction pursuit shift differences less than or equal to half the mean pursuit shift (10.6°) as well as preferred- and null-direction VORC shift differences less than or equal to half the mean VORC shift (9.27°) are plotted with tie lines (—) connecting the preferred- and null-direction occurrences.

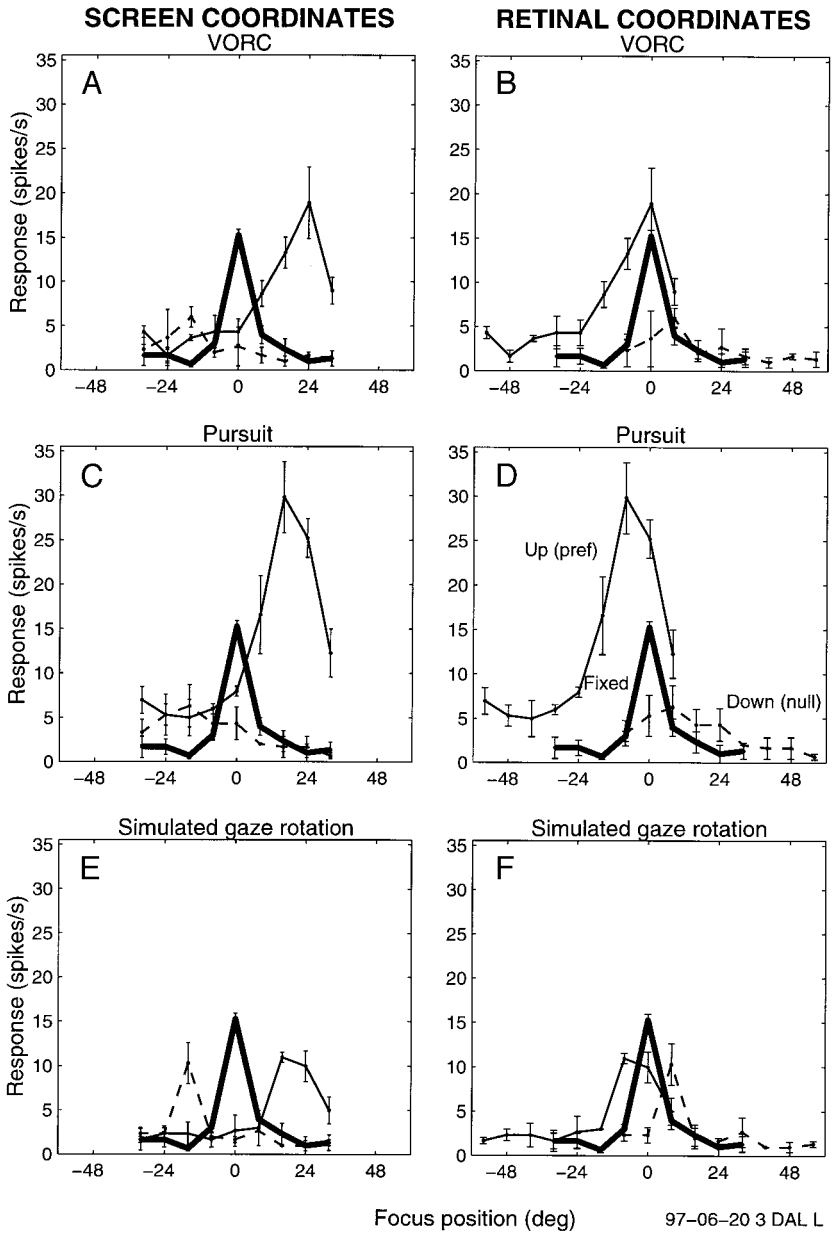

FIG. 11. Response of a single ''retinal,'' gain-modulated neuron in the heading experiment. Focus tuning curves from the 3 gaze tracking conditions (*rows*) are plotted in the coordinates of the screen (*left*) and the retinae (*right*) to help visualize the alignment of key features. Fixed gaze curve (thick solid line) is identical in all panels. Preferred (solid lines) and null (dashed lines) tuning curves are displaced by the theoretical shift offsets of −24 and +24°, respectively, with respect to the fixed gaze curve to plot the curves in retinal coordinates. Preferred-optic-flow pattern is expansion and preferred gaze tracking direction is up. Data points are the means ± SE for 3 replicates.

arrive at a composite view, or working model, of MSTd during gaze rotations. We describe Fig. 10*B* here because of its relation to Fig. 10*A*, but reserve interpretation for the DISCUSSION. Figure 10*B* is the correlation plot from Fig. 10*A* with four subpopulations delineated. The space of VORC compensation versus pursuit compensation can be roughly sectioned into four groups: neurons with little correlation and compensation, neurons with appreciable correlation and compensation, neurons with only appreciable VORC compensation, and neurons with only appreciable pursuit compensation.

GAIN MODULATION. We now ask if MSTd neurons also use gaze-rotation signals, whether retinal, pursuit, or VORC in origin, to gain modulate focus tuning curves. Figure 11 plots focus tuning curves from the heading experiment in the same format as Fig. 8 but with data from a different cell. Comparing these two figures reveals very different alignment patterns. These tuning curve maxima, minima, and inflection points align better in retinal coordinates, than in screen coordinates, for all conditions. ''Retinal,'' or nearly retinal, neurons are characterized by this type of alignment pattern. Figure 11 also shows that VORC and pursuit cues appear to modulate the firing rate. Preferred-direction tuning curves are enhanced while null-direction tuning curves are suppressed with respect to the fixed gaze tuning curve. The simulated gaze rotation condition exhibits less gain modulation.

This neuron shows that gaze-rotation signals can gain modulate focus tuning curves, which happen to align horizontally in near-retinal coordinates. Gain modulation also is found in neurons that align in nonretinal coordinates (e.g., screen coordinates). We quantified gain modulation by horizontally aligning tuning curves, according to their optimal shifts, and calculating the ratio of their average responses. For example, a cell with a mean preferred-direction VORC response of 120 spikes/s and a mean fixed-gaze response of 100 spikes/s, as

calculated from the overlapping focus positions, would have a preferred-direction VORC gain of 1.2 (+20%); a cell with a mean null-direction VORC response of 80 spikes/s and an associated mean fixed-gaze response of 100 spikes/s would have a null-direction VORC gain of 0.8 (−20%).

Figure 12 plots histograms of the gain for all conditions. All distribution parameters and test values are listed in Table 2. For VORC and pursuit, the preferred directions tend to have gain modulations greater than unity (1.22 and 1.51 means, respectively), whereas the null directions tend to have gain modulations of about unity (1.04 and 1.07 means, respectively). Both preferred-direction distributions are significantly greater than unity ($P < 0.001$, Wilcoxon), whereas both null-direction distributions are indistinguishable from unity ($P > 0.05$, Wilcoxon). These results indicate that MSTd neurons use either retinal or gaze-rotation signals to increase responses during preferred-direction gaze rotations. To distinguish the gain modulation effects of the retinal motion (rotational flow) from the effects of the VORC and pursuit cues, we considered the simulated gaze-rotation data. Simulated gaze-rotation distributions are centered close to unity with means of 1.06 for preferred and 1.13 for null directions. Although the preferred direction distribution is not significantly different from unity ($P > 0.05$, Wilcoxon), the null direction is ($P < 0.001$, Wilcoxon). The preferred-direction gain in this condition is far less than the preferred-direction gains in the real gaze rotation conditions, which suggests that VORC and pursuit cues drive the majority of gain modulation.

To more directly investigate the contribution of the VORC and pursuit cues, we examined the cell-by-cell difference between the VORC or pursuit gain modulation and the simulated condition gain modulation. We found that significant gain modulation remained for preferred-direction VORC and pursuit ($P < 0.05$ and $P < 0.001$, Wilcoxon, respectively), confirming that VORC and pursuit cues drive gain beyond levels created by retinal cues alone.

MSTd neurons use VORC and pursuit cues to gain modulate responses. The use of gaze rotation signals to gain modulate visual-motion responses appears to be analogous to how other posterior parietal neurons use gaze position signals to gain modulate visual position responses (Andersen 1997). Many PPC neuron responses are monotonically gain modulated by gaze position, and the resulting gain field is characterized by its gradient, the direction and rate of maximal change. If such a gaze-rotation gain field exists in individual MSTd neurons, then we measured this field at only three velocities, which are analogous to three positions for gaze-position gain fields. We measured the visual response during 9.2°/s gaze rotation in the null direction, during 0°/s gaze rotation (fixed gaze), and during 9.2°/s gaze rotation in the preferred direction. With these three measurements we can only estimate the slope of the gaze-rotation gain field along this one dimension, which falls along the preferred-null axis.

A measure of the slope of the gaze-rotation gain field, along the preferred-null direction, is the difference between the preferred-direction gain modulation and the null-direction gain modulation. Figure 13 plots histograms of this measure on a cell-by-cell basis for all three gaze-rotation conditions. All distribution parameters and test values are listed in Table 2. A cell with a positive preferred-minus-null gain difference has a positive gaze-rotation gain field slope (in the null-to-preferred direction). A population of such cells has a distribution significantly skewed toward values greater than zero and indicates that the population as a whole tends to have a positive slope

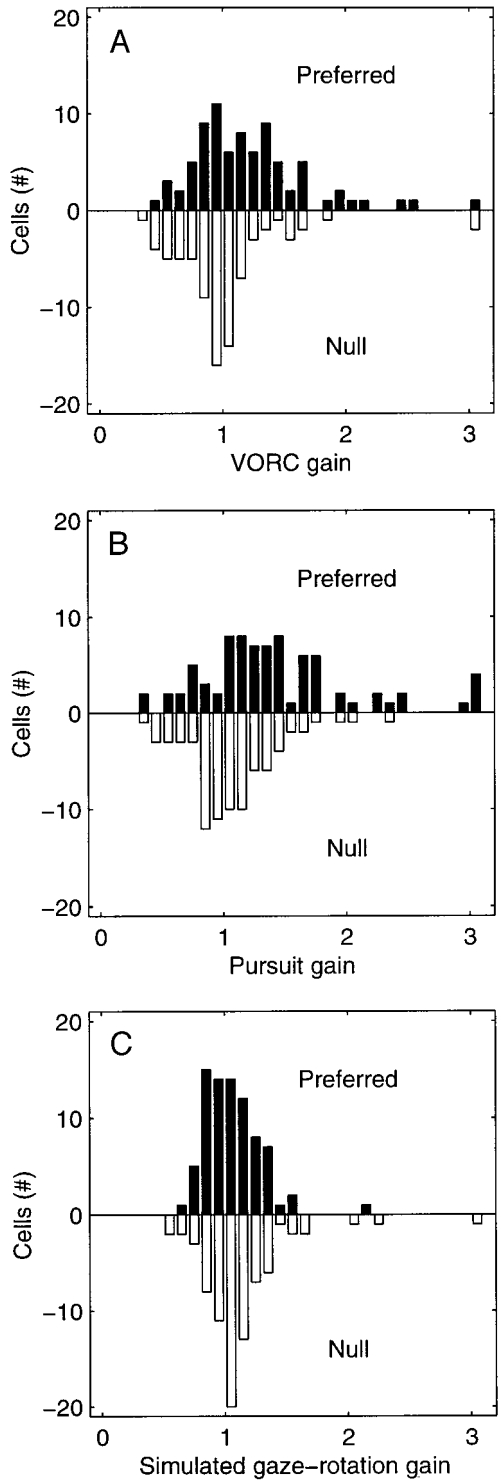

FIG. 12. Histograms of the gain modulation for the 3 gaze rotation conditions. Unity gain modulation indicates that gaze rotation does not modulate the tuning curve, whereas values greater or less than unity indicates that gaze rotation increases or decreases the neuron's response, respectively. *A-C*: histograms of the gain for the VORC, pursuit, and simulated gaze rotation conditions, respectively. Null direction is plotted as downward bars, and the preferred direction is plotted as upward, filled bars. Binwidth is 0.1. All distribution parameters and test values are listed in Table 2.

TABLE 2. *Gain-modulation-related distribution parameters and significance values*

Distribution	Related Figure	25th Percentile	Median	75th Percentile	Wilcoxon, T	Significance	Mean	Mean/Rate, %/(°/s)
Histograms								
Preferred VORC	12*A*	0.90	1.15	1.41	888	$P < 0.001$	1.22	2.43
Null VORC	12*A*	0.80	0.98	1.13	1,458	$P > 0.05$	1.04	0.44
Preferred pursuit	12*B*	1.06	1.31	1.66	474	$P < 0.001$	1.51	5.53
Null pursuit	12*B*	0.85	1.05	1.26	1,342	$P > 0.05$	1.07	0.77
Preferred simulated	12*C*	0.89	1.04	1.18	1,203	$P < 0.05$	1.06	0.69
Null simulated	12*C*	0.96	1.05	1.22	938	$P < 0.001$	1.13	1.43
Preferred VORC − simulated	—	−0.14	0.06	0.33	1,105	$P < 0.05$	0.16	1.75
Null VORC − simulated	—	−0.28	−0.11	0.07	1,024	$P < 0.01$	−0.09	−0.99
Preferred pursuit − simulated	—	−0.11	0.23	0.65	715	$P < 0.001$	0.45	4.85
Null pursuit − simulated	—	−0.29	−0.06	0.17	1,379	$P > 0.05$	−0.06	−0.66
Preferred − null VORC	13*A*	−0.16	0.20	0.50	935	$P < 0.001$	0.18	1.00
Preferred − null pursuit	13*B*	−0.04	0.28	0.64	690	$P < 0.001$	0.44	2.38
Preferred − null simulated	13*C*	−0.26	−0.04	0.15	1,388	$P > 0.05$	−0.07	−0.37
Retinal								
Preferred VORC	14*A*	0.94	1.18	1.43	167	$P < 0.001$	1.32	3.49
Null VORC	14*B*	0.74	0.99	1.10	307	$P > 0.05$	1.04	0.47
Preferred pursuit	14*C*	1.07	1.30	1.72	88	$P < 0.001$	1.47	5.10
Null pursuit	14*D*	0.83	1.07	1.19	203	$P > 0.05$	1.05	0.51
Preferred simulated	14*E*	0.89	1.00	1.13	613	$P > 0.05$	1.04	0.46
Null simulated	14*F*	0.96	1.05	1.17	447	$P < 0.05$	1.06	0.66
Screen								
Preferred VORC	14*A*	0.83	1.06	1.29	59	$P > 0.05$	1.07	0.73
Null VORC	14*B*	0.90	0.99	1.12	148	$P > 0.05$	1.01	0.12
Preferred pursuit	14*C*	0.98	1.29	1.37	27	$P < 0.01$	1.24	2.58
Null pursuit	14*D*	0.85	1.04	1.26	147	$P > 0.05$	1.04	0.47
Preferred simulated	14*E*	0.86	1.04	1.28	53	$P > 0.05$	1.07	0.75
Null simulated	14*F*	0.92	1.06	1.22	27	$P > 0.05$	1.12	1.30

A description of the distribution and the related figure, if any, are listed on rows along with distribution parameters (25%, median, 75%, and mean values) and hypothesis tests values (Wilcoxon *t*-test). Significance values refer to Wilcoxon tests with null hypotheses that the distributions are centered on one or zero VORC-simulated and pursuit-simulated. The mean/rate ratio is defined as the ratio of the distribution mean (%) to the gaze rotation speed range (°/s). VORC, vestibulo-ocular reflex cancellation.

along the null-to-preferred direction. In other words, the visual response increases during preferred-direction gaze rotation and decreases during null-direction gaze rotation in single cells. Figure 13 shows that this is indeed the case for VORC and pursuit. Both distributions are skewed significantly toward positive values ($P < 0.001$, Wilcoxon). The simulated gaze rotation distribution is not significantly different from zero, which is consistent with the previous observation that gain modulation is weak in this condition ($P > 0.05$, Wilcoxon). Dividing the preferred-minus-null distribution means, expressed as percent gain, by the range of rotation speeds (9.2 − −9.2°/s = 18.4°/s) gives a measure of the slope of the gaze-rotation gain field. VORC, pursuit, and simulated conditions have slopes of 1.0, 2.4, and −0.4%/(°/s), respectively. Better estimates of gaze-rotation gain field shapes and slopes requires measuring gain modulation at additional rotation speeds and in additional directions.

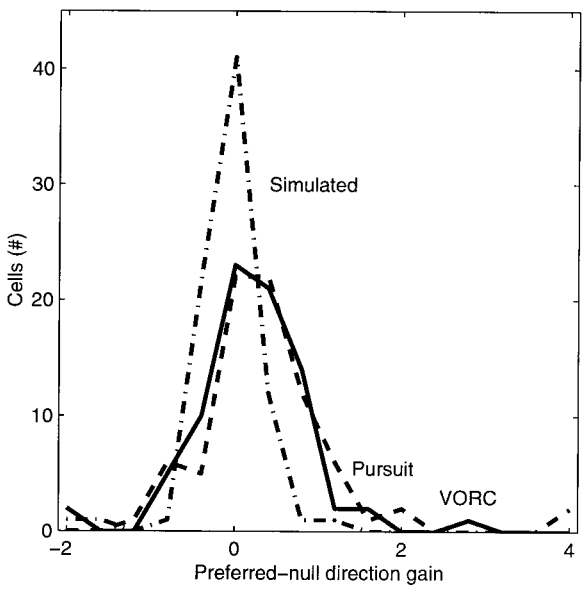

FIG. 13. Histograms of the cell-by-cell difference between the preferred- and null-direction gain modulation in the 3 gaze rotation conditions: VORC (—), pursuit (- - -), and simulated rotation (- · -). Binwidth is 0.4. All distribution parameters and test values are listed in Table 2.

The final similarity between gaze-rotation and gaze-position gain fields that we investigated was the equivalence of the two types of gaze rotation, VORC and pursuit. PPC neurons have similar gains for eye and head position. How similar are the VORC- and pursuit-induced gains? VORC and pursuit both have significantly correlated, cell-by-cell preferred- and null-directions gains ($P < 0.001$, $r_s = 0.399$ and $r_s = 0.404$, Spearman, respectively). The VORC and pursuit gain slopes are correlated on a cell-by-cell basis ($P < 0.01$, $r_s = 0.321$, Spearman). The best fit slope is 0.50 (2-dimensional least means square fit), indicating that on average the VORC gaze-rotation gain field slope is about half the pursuit gaze-rotation gain field slope. This is in qualitative agreement with gaze-position gain field results in PPC (Brotchie et al. 1995; Snyder et al. 1998). The tendency for both VORC and pursuit to gain modulate individual neurons suggests that MSTd encodes, via

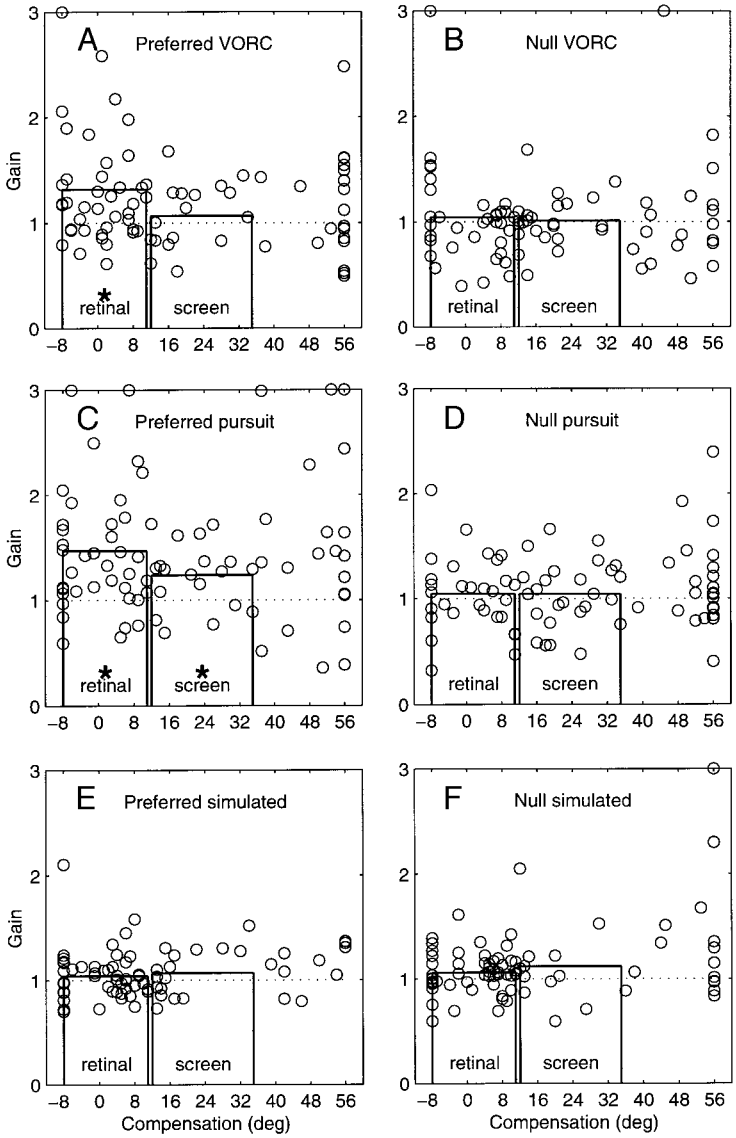

FIG. 14. Correlation plots of gain modulation vs. compensatory shift on a cell-by-cell basis. Preferred (*left*) and null (*right*) directions are considered in each of the 3 gaze rotation conditions (*rows*). Labeled bars indicate mean gains for retinal and screen cells. Means that are significantly different from unity are marked (*). Gains that exceed 3.0 are plotted at 3.0.

gain modulation, both types of gaze rotation although perhaps to differed extents.

SHIFT COMPENSATION AND GAIN MODULATION. So far the gain modulation analysis has considered all cells in the population and did not partition the cells according to their optimal horizontal shifts. However, the functional role of gain perhaps is understood most readily for retinal cells (cells without horizontal shift) where pursuit and VORC cues are combined with retinotopic information. We are now in a position to consider each cell's horizontal shift and gain modulation. Figure 14 plots gain modulation versus optimal shift on a cell-by-cell basis for both gaze-rotation directions and in each of the three gaze-rotation conditions. For comparative purposes, we consider cells with compensatory shifts of −8, 0, and +8° to be in or near retinal coordinates and cells with 16, 24, or 32° shifts to be in or near screen coordinates. Note that while compensatory shifts were determined to within a 1° resolution, we returned to the experimental 8° resolution, set by the FOE spacing, to calculate gain by shifting tuning curves integral multiples of the FOE spacing.

A few gain trends are apparent in retinal cells. First, preferred-direction gains are higher than null-direction gains in both VORC and pursuit conditions (compare retinal gain in Fig. 14, *A* with retinal gain in *B;* similarly *C* with *D*). All distribution parameters and significance test values are listed in Table 2. The mean gains for preferred- and null-direction VORC are 1.32 and 1.04, respectively, and for preferred- and null-direction pursuit are 1.47 and 1.05, respectively. Second, preferred-direction gain is significantly greater than unity during VORC and pursuit ($P < 0.001$, Wilcoxon) while null-direction gains are not. Finally, simulated gaze-rotation gain is weak for both directions, as seen in Fig. 14 *E* and *F*.

Screen-centered heading cells have similar gain trends but generally exhibit weaker gain modulation. Again preferred-direction gains are higher than null-direction gains in both VORC and pursuit conditions (compare screen cells in *A* and *B* and *C* and *D*). The mean gains for preferred- and null-direction VORC are 1.07 and 1.01, respectively, and for preferred- and null-direction pursuit are 1.24 and 1.04, respectively. Preferred-direction retinal cells do not have significantly different gain than preferred-direction screen cells during VORC ($P > 0.05$, Mann-Whitney); this is also true for pursuit ($P > 0.05$,

Mann-Whitney). This is consistent with the general finding that gain modulation and compensatory shifts are not significantly correlated ($P > 0.05$, Spearman, for preferred and null directions in VORC, pursuit, and simulated gaze-rotation conditions considered separately).

These results indicate that gain modulation is stronger in the preferred direction than in the null direction and that gain appears to be weaker in heading cells (screen cells) than in retinal cells although we did not find this trend to be significant.

DISCUSSION

Cortical area MSTd has been implicated as a visual navigation center for the past decade. Many studies have shown that neurons in this area are sensitive to the visual-motion patterns present during locomotion, and we recently demonstrated that MSTd neurons use a pursuit signal to effectively subtract visual-motion artifacts introduced by moving the eyes in the orbits (Bradley et al. 1996). This study asked if MSTd also can contend with visual-motion distortions caused by passive head movements because we typically shift our gaze with head rotations as well as eye rotations. As predicted for a visual navigation center, we found that MSTd receives a signal of vestibular origin (VORC signal) and uses this signal to compensate, at least partly, for the rotational flow added by rotating the head in the world. This is accomplished by adjusting a neuron's focus tuning curve so that it becomes maximally sensitive to the sum of the preferred motion pattern in the world and the rotational flow added by the gaze rotation. In this way, many neurons remain maximally sensitive to heading. It appears that considerable compensation also can be driven by retinal cues alone.

We also found that most MSTd neurons receive both pursuit and VORC signals and that these signals are similar in a given cell. Moreover, many neurons use these signals to similarly compensate for eye and head rotations. However, not all MSTd neurons adjust their focus tuning so as to become invariant to gaze rotations. Although most cells do compensate at least partly, those that remain in retinal coordinates are substantially gain-modulated by both pursuit and VORC signals. These cells could converge to form the inputs to heading cells as we have suggested previously (Bradley et al. 1996) or could form a distributed representation of heading as other PPC neurons do or both. Area MSTd receives an exquisite convergence of retinal and extraretinal signals that enable neurons to encode heading even during eye and head rotations. These results suggest strongly that MSTd plays a central role in heading computation and perception in primates.

Comparison of pursuit and VORC signals

The preferred-direction experiment explored the influence of pursuit and VORC signals, or cues, on visual responses. However, we cannot be sure of the exact nature of the pursuit and VORC signals. A pure pursuit signal may reflect an eye-muscle proprioceptive signal or, more likely, an efference copy of an eye movement command and such a signal is known to exist in MSTd (Newsome et al. 1988). A pure VORC signal, as discussed in the INTRODUCTION, may be a vestibular signal, an eye-movement signal, or more likely a combination of both. The origin of these signals is extraretinal. In the preferred-direction experiment, we moved the preferred-optic-flow stimulus with the pursuit and VORC targets, and we measured the modulatory effects of the extraretinal signals on the cell's visual response. The presence of the optic-flow pattern raises the possibility that less than perfect pursuit and VORC could contribute a sizable retinal slip signal to the measured response, which would otherwise consist of just the optic-flow visual response and the extraretinal signal. Although we confirmed that the monkeys pursued and canceled the VOR quite accurately, we cannot rule out this possibility completely. Another observation also suggests that we selected an axis close to the true, extraretinally based preferred-null axis. Just before the optic-flow stimulus appeared, the monkey pursued or VORC-tracked a single point in an otherwise dark room. This response tended to be greater in preferred-direction pursuit and VORC than in the null direction (compare prestimulus periods in Fig. 7).

Pursuit and VORC signals tended to be tuned for ipsilateral and downward gaze rotation (Fig. 6*A*), although only the pursuit trend is significant. Downward gaze rotation is intriguing because it is consistent with a role in visual navigation, where tracking objects on the ground while moving forward often leads to downward gaze rotations. This bias is reminiscent of the overrepresentation of expansion cells in MSTd; this presumably is related to our habit of looking along our heading path, which causes expanding retinal flow (Graziano et al. 1994).

Individual MSTd neurons also tend to be selective for a given direction of gaze rotation regardless of whether gaze rotation is produced by eye or passive-head rotation (Fig. 6*B*). This suggests that MSTd may encode the direction of total gaze rotation. If VORC signals also are tuned for the speed of gaze rotation, as is the case for pursuit signals, then it is possible that total gaze velocity also is encoded in MSTd (Kawano et al. 1980, 1984; Shenoy et al. 1998). It is also possible that other important extraretinal signals are present in MSTd. Natural head turns, in contrast with the VORC paradigm that rotates the entire animal, are accompanied by proprioceptive signals from neck muscles and joints and efference copy of head-turn motor commands. Although the VORC signal alone, which derives from the vestibular canals, clearly encodes passive head movements, it is possible that proprioceptive and efference copy signals serve additional roles in reporting the metrics of active head movements.

Shift compensation

Many MSTd neurons are able to maintain their selectivity for visual-motion patterns in the world despite large retinal image changes caused by gaze rotations (Fig. 8). This is achieved by shifting their retinal-focus position sensitivity. Such dynamic adaptation is critical for seeing motion in the world independent of ego motion, and this perceptual constancy allows us to navigate through our environment while moving our eyes and head. But how is this dynamic adaptation achieved?

There appear to be at least two possibilities. First, for a neuron to remain tuned for a central FOE in the world during rightward gaze rotation, the retinal tuning must become more responsive to rightward foci and less responsive to central foci

(Fig. 1). This dynamic adaptation could occur in the projections from area MT, which extracts unidirectional motion within small receptive fields, to area MSTd. Dynamically strengthening connections from some MT cells, while weakening connections from others, effectively changes the preferred visual-motion pattern of the afferent MSTd neuron. It is plausible that extraretinal gaze-rotation signals selectively strengthen and weaken these connections in a pattern appropriate for the current gaze rotation. As recognized by Perrone and Stone (1994, 1998), incorporating this type of dynamic adaptation into a template model of MSTd should reduce drastically the total number of neurons needed to accurately encode heading during gaze rotations.

A second possibility is that dynamic adaptation occurs within MSTd. In this scheme, MT-to-MSTd connectivity remains constant, and each compensating (heading) MSTd neuron receives input from at least two noncompensating (retinal) MSTd neurons as we recently proposed (Bradley et al. 1996). In this architecture, a heading cell sums the output of retinal cells, the preferred focus positions of which are mutually offset. Extraretinal gaze-rotation signals selectively enhance (gain modulate up) and suppress (gain modulate down) the output of retinal cells in a pattern appropriate for the current gaze rotation. For example, enhancing retinal cells tuned for rightward foci and suppressing retinal cells tuned for central foci effectively shifts the heading cell's focus tuning rightward as needed during rightward gaze rotation. Although our data certainly do not rule out the ''MT-to-MSTd'' mechanism, it does appear consistent with the ''within-MSTd'' mechanism because two important, predicted MSTd response features were observed: the existence of compensating (Fig. 8) and noncompensating (Fig. 11) neurons and the existence of gain-modulated retinal cells (Fig. 14, *A* and *C*).

The heading experiment also demonstrates that neurons can use retinal cues, not just pursuit and VORC cues, to compensate at least partly. We did not find this to be the case in our previous heading study, which used large optic-flow stimuli and a higher pursuit speed (Bradley et al. 1996). There are at least three possible reasons for this discrepancy. First, comparing the mean simulated gaze-rotation compensation for the $18 \times 18°$ stimulus frame ($12.47°/24° = 52.0\%$; Fig. 9*B*) with the mean compensation for a $50 \times 50°$ stimulus frame ($-1°/30° = -3.3\%$) (Bradley et al. 1996) suggests that retinal-based compensation may increase as the stimulus frame becomes more visible to the receptive field. In other words, the stimulus edges in our experiments are well within the receptive field and could provide an accurate cue as to the direction and speed of gaze rotation. Larger stimuli provide less of a cue because the edges fall on the lower sensitivity periphery of the receptive field. Second, it is possible that the faster rotation rate used in the previous experiment (15.7 vs. 9.2°/s) led to lower levels of compensation because the faster visual motion was beyond the neurons' optimal speed range, though this seems unlikely given the broad speed tuning in MSTd.

Finally, Komatsu and Wurtz (1988b) found that the preferred direction of visual motion reverses as the size of the stimulus field increases. Moreover, the size of the stimulus field leading to reversal of the preferred direction increases as the speed of visual-motion increases. Last, the vast majority of cells have preferred directions of motion for large stimulus fields opposite to the preferred-pursuit directions. Taken together, it is possible that compensation is greater in the present experiment because the choice of rotation rate and visual-stimulus size caused most MSTd neurons to have their preferred-motion direction aligned opposite to the preferred gaze-rotation direction, which is necessary for retinal and pursuit/VORC cues to constructively combine and drive compensation, whereas the previous experiment (Bradley et al. 1996) operated in the opposite regime. Preliminary data from 30 neurons in *monkey DAL* indicate that most MSTd cells do have oppositely aligned preferred visual-motion directions and preferred-pursuit directions with stimulus size and rotation rates similar to those used in the current experiments (K. V. Shenoy, J. A. Crowell, and R. A. Andersen, unpublished observation).

In addition to the strong compensatory shifts in the population, many individual MSTd neurons have similar degrees of VORC- and pursuit-induced compensation. A subset of neurons also have similar preferred- and null-direction shifts and therefore report heading regardless of the type of gaze rotation and regardless of the direction of rotation (Fig. 10*B*, tie lines). However, not all neurons have well-correlated shifts, and the space of VORC compensation versus pursuit compensation can be sectioned roughly into four groups as shown in Fig. 10*B*. It is possible that either the entire MSTd population is read out by down stream cortical areas or that subpopulations serve different roles in various behavioral conditions. Human psychophysical studies may help interpret the role of MSTd and its subpopulations in visual navigation (see *Relationship among physiology, psychophysics, and models*).

Gain modulation

In the population, preferred-direction pursuit and VORC significantly modulate visual responses. These results bear close resemblance to gain modulation in PPC caused by gaze position signals (Andersen and Mountcastle 1983; Andersen et al. 1985, 1990; Brotchie et al. 1995; Snyder et al. 1998). It is possible that the brain uses a common mechanism (gain modulation) for combining similar types of information.

Figure 15 illustrates two systems, with a common gain mechanism, for combining gaze-rotation and visual-motion information (gaze-rotation gain field system) and for combining gaze-position and visual-position information (gaze-position gain field system). Figure 15, *top*, illustrates the analogy between the addition of eye and head rotation information to retinal motion information to encode motion in the world (*A*) and the addition of eye and head position information to retinal position information to encode position in the world (*B*). The signals in the two systems are related simply by a single temporal derivative. After the retinal effects of gaze rotation have been taken into account, the absolute position of the focus of expansion, which can be thought of as a visual object, must be encoded. The open arrow passing information from the motion system to the position system in Fig. 15 suggests such a processing hierarchy (e.g., MSTd projects to areas 7A and VIP, which encode target locations). It is also possible that MSTd simultaneously encodes the position of motion patterns in the world by employing eye position signals, which have recently been reported, and head position signals, which also may exist (Bremmer et al. 1997; Squatrito and Maioli 1996).

Figure 15, *bottom*, illustrates the common gain mechanism

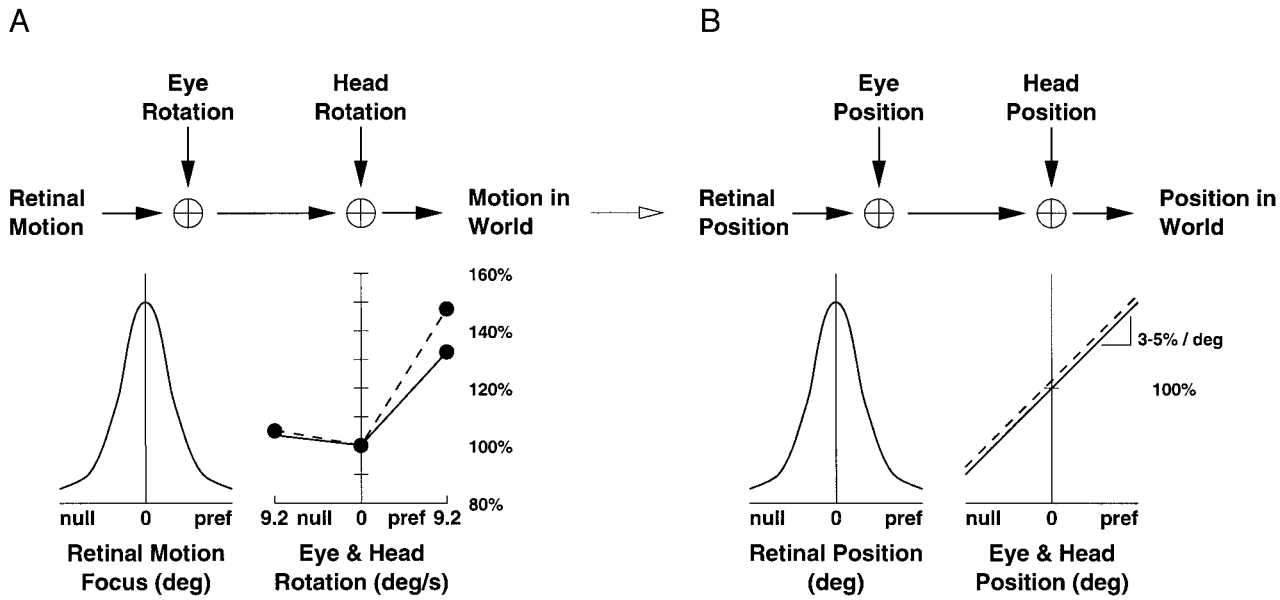

FIG. 15. Two system diagrams, with a common mechanism, for combining gaze rotation and visual motion information (gaze-rotation gain field system) and for combining gaze position and visual position information (gaze-position gain field system). *Top*: analogy between the addition of eye and head rotation information to retinal motion information to encode motion (FOE) in the world regardless of gaze rotation (*A*) and addition of eye and head position information to retinal position information to encode position in the world regardless of gaze position (*B*). *Bottom*: gain mechanism by which the motion system combines focus tuning curves with gaze rotation signals (*A*) and by which the position system combines retinal position signals and gaze position signals (*B*).

by which the motion system combines retinal motion signals with gaze rotation signals and by which the position system combines retinal position signals and gaze position signals. In the motion system (*A*), a retinal focus tuning curve is modulated by a function of eye or head rotation. The pursuit and VORC gain data are the mean gains from retinal cells (see Table 2) and have slopes of 5.10 and 3.49%/(°/s), respectively, in the preferred direction. Whereas gain appears to be a half-wave rectified version of the rotation rate, data from intermediate rotation speeds are required to determine the true gain curve. The position system (*B*) has been well characterized and retinotopic visual responses are modulated by monotonic functions of eye or head position. Typical gain slopes are 3–5%/° and enhance as well as suppress activity relative to the levels present in the forward gaze position (Brotchie et al. 1995; Snyder et al. 1998). Gain fields enable a population of neurons to encode, in a distributed representation, the focus of expansion regardless of gaze rotation (*A*, gaze-rotation gain field) and absolute position information could readily be added to this representation by the position system (*B*, gaze-position gain field). It is also possible that individual MSTd heading neurons, which have removed the retinal effects of gaze rotation, either project to the positional system or also include gaze-position effects.

Relationship among physiology, psychophysics, and models

Accurate heading perception depends on our ability to correctly interpret visual motion even while rotating our gaze. A recent modeling study (Lappe 1998) successfully reproduced human psychophysical and monkey neurophysiological data (Bradley et al. 1996) during pursuit by incorporating an extraretinal pursuit signal. Based on results from this model, Lappe (1998) proposed that extraretinal compensation for eye movements does not need to be perfect in single neurons to estimate heading accurately. With the present findings that VORC compensation is nearly as complete as pursuit compensation and that individual cells compensate for both types of gaze rotation, we would expect this model to easily extend to include head turns.

Similar results also should be possible with template models if extraretinal signals are allowed to dynamically adapt motion templates (Perrone and Stone 1994, 1998). Finally a model that gain-modulates retinotopic visual responses with pursuit velocity signals, similar to models of the PPC position system, successfully has described a distributed representation of heading (Beintema and van den Berg 1998; Bradley et al. 1996; van den Berg and Beintema 1997; Zipser and Andersen 1988).

New considerations are how MSTd encodes heading during eye and/or head rotations and how this representation is read out. This study and recent human psychophysical investigations suggest that MSTd plays a central role in heading perception but that MSTd may not be the final perceptual locus. Humans correctly report their self-motion during simulated translations over ground planes during fixation, pursuit, and active head pursuit, which uses a VORC paradigm (Crowell et al. 1998a; Royden et al. 1992). Although a VORC signal is present during active head pursuit, and potentially contributes to heading judgments, humans make large heading errors when only a VORC signal is present, measured in a passive VORC condition that matches our physiology paradigm (Crowell et al. 1998a,b using wall displays). Performance also is reduced when the VORC signal is absent during active head pursuit, measured by passively rotating the body but actively counter-rotating the head so as to keep it stationary in space (mean compensation of 68%) (Crowell et al. 1998a). Together these

results imply that the VORC signal is necessary but not sufficient for accurate heading estimates.

These psychophysical experiments indicate that while heading perception is nearly perfect during pursuit, perceptual accuracy is significantly reduce during passive VORC (Crowell et al. 1998a). One hypothesis is that the lower level of gain modulation observed during passive VORC, as compared with the level of gain modulation during pursuit, reflects this reduced perceptual accuracy. Additional gain from proprioceptive and efference signals could raise the level of gain modulation and thereby account for the excellent performance during active head pursuit.

Another, and possibly more likely, hypothesis is that even though shift compensation is similar in individual neurons during pursuit and passive VORC conditions, MSTd subpopulations (Fig. 10*B*) may be selectively read out and thereby account for psychophysical performance. One possibility is that only neurons that compensate exclusively during pursuit (region d) contribute to perception. This seems unlikely because there are few neurons in this category (10%) and because there is a similar fraction of neurons that compensate only during passive VORC (region c), which have no known perceptual role. A more likely possibility is that a downstream area selects which MSTd subpopulation to read out based on a more complete set of extraretinal signals (e.g., proprioceptive and efference signals). For example, although VORC and pursuit signals create the entire representation shown in Fig. 10*B*, the compensating subpopulation (region b) may be read out only during eye pursuit and active head turns, whereas the noncompensating subpopulation (region a) may be read out during passive head turns. This suggests that the brain may have adopted the strategy of using a small, possibly minimal, number of gaze rotation signals (e.g., pursuit and VORC) to create a neural representation but a larger, possibly complete, set of extraretinal signals to selectively read out, or interpret, the representation.

We thank Drs. K. L. Grieve, L. H. Snyder, J. A. Crowell, and M. S. Banks for scientific discussions; Dr. K. L. Grieve and B. Gillikin for technical assistance; Drs. L. H. Snyder and K. L. Grieve for designing and helping test the vestibular chair; M. Sahani for developing the real-time control software HYDRA; Drs. J. A. Crowell, L. H. Snyder, and Y. E. Cohen for valuable comments on this manuscript; and C. Reyes for administrative assistance.

This work was supported in part by National Eye Institute (NEI) Grant EY-07492, NEI postdoctoral grant EY-06752 to K. V. Shenoy, the Sloan Foundation for Theoretical Neurobiology at the California Institute of Technology, the Office of Naval Research, and the Human Frontiers Scientific Program.

Present address of D. C. Bradley: Dept. of Psychology, University of Chicago, Chicago, IL 60637.

Address for reprint requests: R. A. Andersen, Mail Code 216–76, Division of Biology, California Institute of Technology, Pasadena, CA 91125.

Received 15 June 1998; accepted in final form 22 January 1999.

REFERENCES

ANDERSEN, R. A. Multimodal integration for the representation of space in the posterior parietal cortex. *Philos. Trans. R. Soc. Lond. B Biol. Sci.* 352: 1421–1428, 1997.

ANDERSEN, R. A., BRACEWELL, R. M., BARASH, S., GNADT, J. W., AND FOGASSI, L. Eye position effects on visual, memory, and saccade-related activity in areas LIP and 7a of macaque. *J. Neurosci.* 10: 1176–1196, 1990.

ANDERSEN, R. A., BRADLEY, D. C., AND SHENOY, K. V. Neural mechanisms for heading and structure-from-motion perception. *Cold Spring Harbor Symp. Quant. Biol.* 61: 15–25, 1996.

ANDERSEN, R. A., ESSICK, G. K., AND SIEGEL, R. M. Encoding of spatial location by posterior parietal neurons. *Science* 230: 456–485, 1985.

ANDERSEN, R. A. AND MOUNTCASTLE, V. B. The influence of the angle of gaze upon the excitability of the light sensitive neurons of the posterior parietal cortex. *J. Neurosci.* 3: 532–548, 1983.

BEINTEMA, J. A. AND VAN DEN BERG, A. V. Heading detection using motion templates and eye velocity gain fields. *Vision Res.* 38: 2155–2179, 1998.

BRADLEY, D. C., MAXWELL, M. A., ANDERSEN, R. A., BANKS, M. S., AND SHENOY K. V. Neural mechanisms for heading perception in primate visual cortex. *Science* 273: 1544–1547, 1996.

BREMMER, F., ILG, U. J., THIELE, A., DISTLER, C., AND HOFFMANN K.-P. Eye position effects in monkey cortex. I. Visual and pursuit-related activity in extrastriate areas MT and MST. *J. Neurophysiol.* 77: 944–961, 1997.

BRITTEN, K. H. Clustering of response selectivity in the medial superior temporal area of extrastriate cortex in the macaque monkey. *Vis. Neurosci.* 15: 553–558, 1998.

BRITTEN, K. H. AND VAN WEZEL, J. A. Electrical microstimulation of cortical area MST biases heading perception in monkeys. *Nat. Neurosci.* 1: 59–63, 1998.

BROTCHIE, P. R., ANDERSEN, R. A., SNYDER, L. H., AND GOODMAN, S. J. Head position signals used by parietal neurons to encode locations of visual stimuli. *Nature* 375: 232–235, 1995.

CELEBRINI, S. AND NEWSOME, W. T. Microstimulation of extrastriate area MST influences performance on a direction discrimination task. *J. Neurophysiol.* 73: 437–448, 1995.

CROWELL, J. A., BANKS, M. S., SHENOY, K. V., AND ANDERSEN, R. A. Visual self-motion perception during head turns. *Nat. Neurosci.* 1: 732–737, 1998a.

CROWELL, J. A., MAXWELL, M. A., SHENOY, K. V., AND ANDERSEN, R. A. Retinal and extra-retinal motion signals both affect the extent of gaze-shift compensation (Abstract). *Invest. Ophthalmol. Vis. Sci.* 39: 1093, 1998b.

CULLEN, K. E., BELTON, T., AND MCCREA, R. A. A nonvisual mechanism for voluntary cancellation of the vestibuloocular reflex. *Exp. Brain Res.* 83: 237–252, 1991.

CULLEN, K. E. AND MCCREA, R. A. Firing behavior of brain-stem neurons during voluntary cancellation of the horizontal vestibuloocular reflex. I. Secondary vestibular neurons. *J. Neurophysiol.* 70: 828–843, 1993.

CULLEN, K. E., CHENHUANG, C. J., AND MCCREA, R. A. Firing behavior of brain-stem neurons during voluntary cancellation of the horizontal vestibuloocular reflex. II. Eye-movement related neurons. *J. Neurophysiol.* 70: 844–856, 1993.

DUFFY, C. J. MST neurons respond to optic flow and translational movement. *J. Neurophysiol.* 80: 1816–1827, 1998.

DUFFY, C. J. AND WURTZ, R. H. Sensitivity of MST neurons to optic flow stimuli. I. A continuum of response selectivity to large-field stimuli. *J. Neurophysiol.* 65: 1329–1345, 1991a.

DUFFY, C. J. AND WURTZ, R. H. Sensitivity of MST neurons to optic flow stimuli. II. Mechanisms of response selectivity revealed by small-field stimuli. *J. Neurophysiol.* 65: 1346–1359, 1991b.

DUFFY, C. J. AND WURTZ, R. H. Response of monkey MST neurons to optic flow stimuli with shifted centers of motion. *J. Neurosci.* 15: 5192–5208, 1995.

DUFFY, C. J. AND WURTZ, R. H. Medial superior temporal area neurons respond to speed patterns in optic flow. *J. Neurosci.* 17: 2839–2851, 1997.

ERICKSON, R. C. AND THIER, P. A neuronal correlate of spatial stability during periods of self-induced visual-motion. *Exp. Brain Res.* 86: 608–616, 1991.

ERICKSON, R. C. AND THIER, P. Responses of direction-selective neurons in monkey cortex to self-induced visual-motion. *Ann. NY Acad. Sci.* 656: 766–774, 1992.

FISHER, N. I. *Statistical Analysis of Circular Data.* New York, NY: Cambridge, 1993.

GEESAMAN, B. J. AND ANDERSEN, R. A. The analysis of complex motion patterns by form/cue invariant MSTd neurons. *J. Neurosci.* 16: 4716–4732, 1996.

GEESAMAN, B. J., BORN, R. T., ANDERSEN, R. A., AND TOOTELL, R. B. H. Maps of complex motion selectivity in the superior temporal cortex of alert macaque monkey: a double-label 2-deoxyglucose study. *Cereb. Cortex* 7: 749–757, 1997.

GIBSON, J. J. *The Perception of the Visual World.* Boston, MA: Houghton Mifflin, 1950.

GRAZIANO, M.S.A., ANDERSEN, R. A., AND SNOWDEN, R. J. Tuning of MST neurons to spiral motions. *J. Neurosci.* 14: 54–67, 1994.

JUDGE, S. J., RICHMOND, B. J., AND CHU, F. C. Implantation of magnetic search coils for measurement of eye position: an improved method. *Vision Res.* 20: 535–538, 1980.

KAWANO, K., SASAKI, M., AND YAMASHITA, M. Vestibular input to visual tracking neurons in the posterior parietal association cortex of the monkey. *Neurosci. Lett.* 17: 55–60, 1980.

KAWANO, K., SASAKI, M., AND YAMASHITA, M. Response properties of neurons in posterior parietal cortex of monkey during visual-vestibular stimulation. I. Visual tracking neurons. *J. Neurophysiol.* 51: 340–351, 1984.

KAWANO, K., SHIDARA, M., WATANABE, Y., AND YAMANE, S. Neural activity in cortical area MST of alert monkey during ocular following responses. *J. Neurophysiol.* 71: 2305–2324, 1994.

KOMATSU, H. AND WURTZ, R. H. Relation of cortical areas MT and MST to pursuit eye-movements. I. Localization and visual properties of neurons. *J. Neurophysiol.* 60: 580–603, 1988a.

KOMATSU, H. AND WURTZ, R. H. Relation of cortical areas MT and MST to pursuit eye-movements. III. Interaction with full-field visual stimulation. *J. Neurophysiol.* 60: 621–644, 1988b.

KOMATSU, H. AND WURTZ, R. H. Modulation of pursuit eye movements by stimulation of cortical areas MT and MST. *J. Neurophysiol.* 62: 31–47, 1989.

LAGAE, L., MAES, H., RAIGUEL, S., XIAO, D. K., AND ORBAN, G. A. Responses of macaque STS neurons to optic flow components—a comparison of MT and MST. *J. Neurophysiol.* 71: 1597–1626, 1994.

LAPPE, M. A model of the combination of optic flow and extraretinal eye-movement signals in primate extrastriate visual-cortex—neural model of self-motion from optic flow and extraretinal cues. *Neural Networks* 11: 397–414, 1998.

LAPPE, M., BREMMER, F., PEKEL, M., THIELE, A., HOFFMANN, K.-P. Optic flow processing in monkey STS: a theoretical and experimental approach. *J. Neurosci.* 16: 6265–6585, 1996.

MAUNSELL, J.H.R. AND NEWSOME, W. T. Visual processing in monkey extrastriate cortex. *Annu. Rev. Neurosci.* 10: 363–402, 1987.

NEWSOME, W. T., WURTZ, R. H., AND KOMATSU, H. Relation of cortical areas MT and MST to pursuit eye-movements. II. Differentiation of retinal from extraretinal inputs. *J. Neurophysiol.* 60: 604–620, 1988.

ORBAN, G. A., LAGAE, L., VERRI, A., RAIGUEL, S., XIAO, D., MAES, H., AND TORRE, V. First-order analysis of optical flow in monkey brain. *Proc. Natl. Acad. Sci. USA* 89: 2595–2599, 1992.

PERRONE, J. A. Model for the computation of self-motion in biological-systems. *J. Opt. Soc. Am.* 9: 177–194, 1992.

PERRONE, J. A. AND STONE, L. S. A model of self-motion estimation within primate extrastriate visual-cortex. *Vision Res.* 34: 2917–2938, 1994.

PERRONE, J. A. AND STONE, L. S. Emulating the visual receptive-field properties of MST neurons with a template model of heading estimation. *J. Neurosci.* 18: 5958–5975, 1998.

RAIGUEL, S., VAN HULLE, M. M., XIAO, D.-K., MARCAR, V. L., LAGAE, L., AND ORBAN, G. A. Size and shape of receptive fields in the medial superior temporal area (MST) of the macaque. *Neuroreport* 8: 2803–2807, 1997.

ROBINSON, D. A method of measuring eye movement using a scleral search coil in a magnetic field. *IEEE Trans. Biomed. Eng.* 10: 137–145, 1963.

ROY, J. P., KOMATSU, H., AND WURTZ, R. H. Disparity sensitivity of neurons in monkey extrastriate area MST. *J. Neurosci.* 12: 2478–2492, 1992.

ROY, J. P. AND WURTZ, R. H. The role of disparity-sensitive cortical-neurons in signaling the direction of self-motion. *Nature* 348: 160–162, 1990.

ROYDEN, C. S., BANKS, M. S., AND CROWELL, J. A. The perception of heading during eye movements. *Nature* 360: 583–585, 1992.

ROYDEN, C. S., CROWELL, J. A., AND BANKS, M. S. Estimating heading during eye movements. *Vision Res.* 34: 3197–3214, 1994.

SAKATA, H., SHIBUTANI, H., ITO, Y., TSURUGAI, K., MINE, S., AND KUSUNOKI, M. Functional properties of rotation-sensitive neurons in the posterior parietal association cortex of the monkey. *Exp. Brain Res.* 101: 183–202, 1994.

SAKATA, H., SHIBUTANI, H., KAWANO, K., AND HARRINGTON, T. Neural mechanisms of space vision in the parietal association cortex of the monkey. *Vision Res.* 25: 453–463, 1985.

SAITO, H., YUKIE, M., TANAKA, K., HIKOSAKA, K., FUKADA, Y., AND IWAI, E. Integration of direction signals of image motion in the superior temporal sulcus of the macaque monkey. *J. Neurosci.* 6: 145–157, 1986.

SHENOY, K. V., BRADLEY, D. C., AND ANDERSEN, R. A. Heading computation during head movements in macaque cortical area MSTd. *Soc. Neurosci. Abstr.* 22: 1692, 1996.

SHENOY, K. V., CROWELL, J. A., AND ANDERSEN, R. A. The influence of pursuit speed upon the representation of heading in Macaque cortical area MSTd. *Soc. Neurosci. Abstr.* 24: 1746, 1998.

SHENOY, K. V., CROWELL, J. A., BRADLEY, D. C., AND ANDERSEN, R. A. Perception and neural representation of heading during gaze-rotation. *Soc. Neurosci. Abstr.* 23: 15, 1997.

SNYDER, L. H., GRIEVE, K. L., BROTCHIE, P., AND ANDERSEN, R. A. Separate body-referenced and world-referenced representations of visual space in parietal cortex. *Nature* 394: 887–891, 1998.

SQUATRITO, S. AND MAIOLI, M. G. Gaze field properties of eye position neurones in areas MST and 7a of the macaque monkey. *Vis. Neurosci.* 13: 385–398, 1996.

SQUATRITO, S. AND MAIOLI, M. G. Encoding of smooth pursuit direction and eye position by neurons of area MSTd of macaque monkey. *J. Neurosci.* 17: 3847–3860, 1997.

TANAKA, K., FUKADA, Y., AND SAITO, H. A. Underlying mechanisms of the response specificity of expansion/contraction and rotation cells in the dorsal part of the medial superior temporal area of the macaque monkey. *J. Neurophysiol.* 62: 642–656, 1989.

TANAKA, K., HIKOSAKA, K., SAITO, H., YUKIE, M., FUKADA, Y., AND IWAI, E. Analysis of local and wide-field movements in the superior temporal visual areas of the macaque monkey. *J. Neurosci.* 6: 134–144, 1986.

TANAKA, K. AND SAITO, H. A. Analysis of motion of the visual field by direction, expansion/contraction, and rotation cells clustered in the dorsal part of the medial superior temporal area of the macaque monkey. *J. Neurophysiol.* 62: 626–641, 1989.

THIER, P. AND ERICKSON, R. C. Vestibular input to visual-tracking neurons in area MST of awake rhesus-monkeys. *Ann. NY Acad. Sci.* 656: 960–963, 1992a.

THIER, P. AND ERICKSON, R. C. Responses of visual tracking neurons from cortical area MST-1 to visual, eye and head motion. *Eur. J. Neurosci.* 4: 539–553, 1992b.

TOMLINSON, R. D. AND ROBINSON, D. A. Signals in vestibular nucleus mediating vertical eye movements in the monkey. *J. Neurophysiol.* 51: 1121–1136, 1984.

VAN DEN BERG, A. V. AND BEINTEMA, J. A. Motion templates with eye velocity gain fields for transformation of retinal to head centric flow. *Neuroreport* 8: 835–840, 1997.

WARREN, W. H. *Self-Motion: Visual Perception and Visual Control.* New York: Academic, 1995.

WARREN, W. H. AND HANNON, D. J. Direction of self-motion is perceived from optical flow. *Nature* 336: 162–163, 1988.

WILSON, V. J. AND JONES, G. M. *Mammalian Vestibular Physiology.* New York: Plenum, 1979.

ZIPSER, D. AND ANDERSEN, R. A. A back-propagation programmed network that simulates response properties of a subset of posterior parietal neurons. *Nature* 331: 679–684, 1988.